

# Substantial cold bias during wintertime cold extremes in the southern Cascadia region in historical CMIP6 simulations

Matt Rogers<sup>1</sup>, Guillaume Sadler Mauger<sup>2</sup>, and Nicoleta Cristea<sup>3</sup>

<sup>1</sup>University of Washington Climate Impacts Group

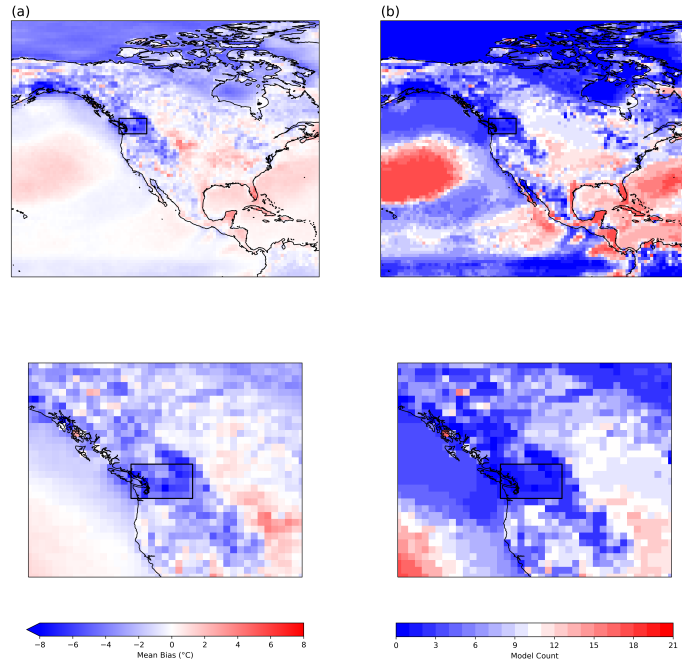
<sup>2</sup>UW Climate Impacts Group

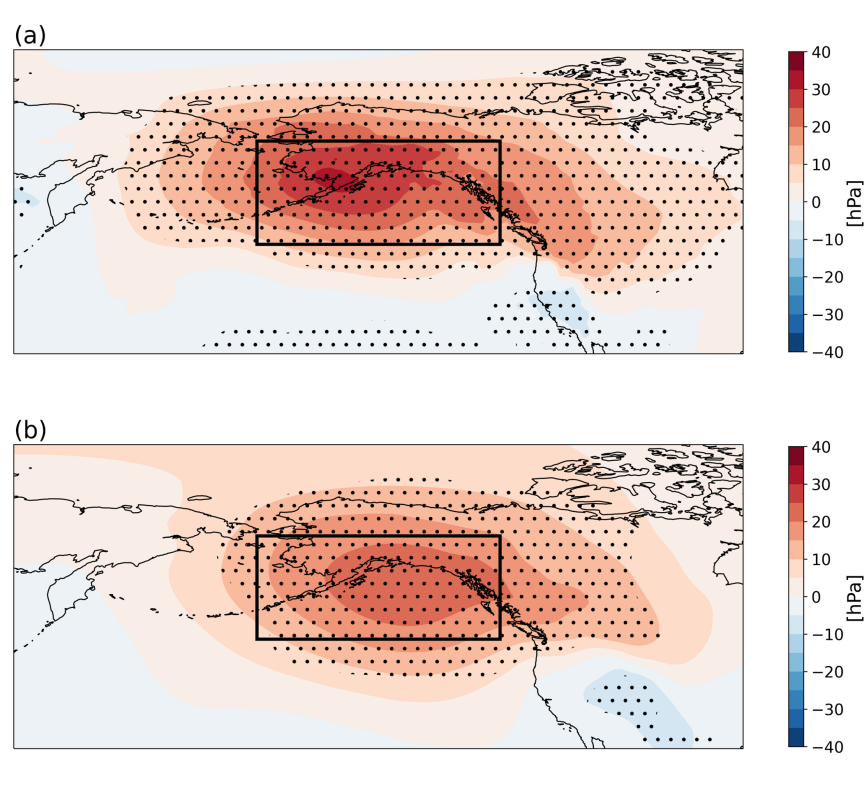
<sup>3</sup>University of Washington, Department of Civil and Environmental Engineering

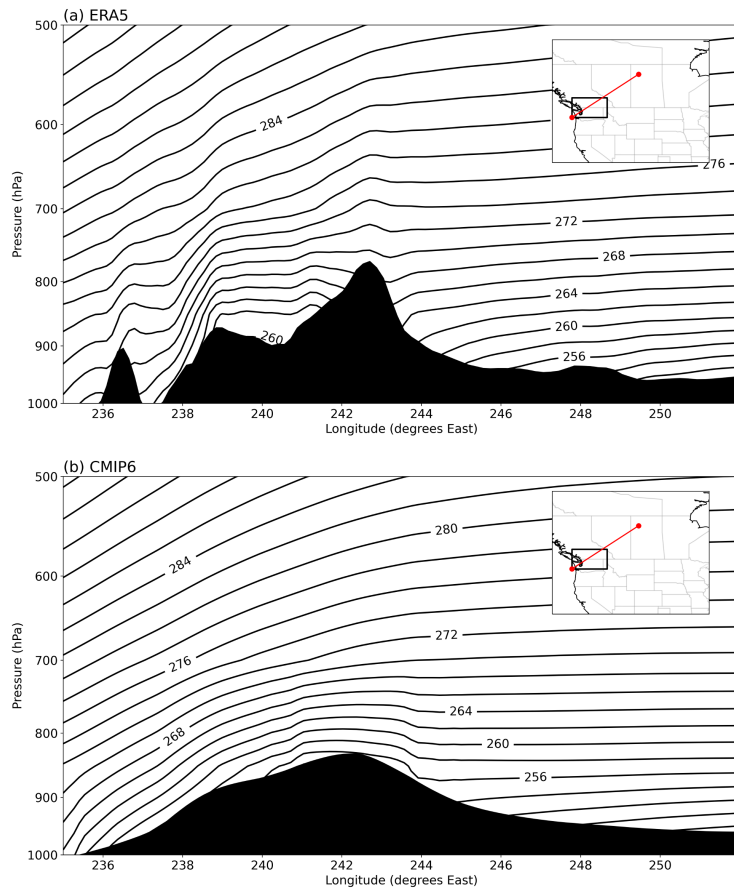
December 21, 2022

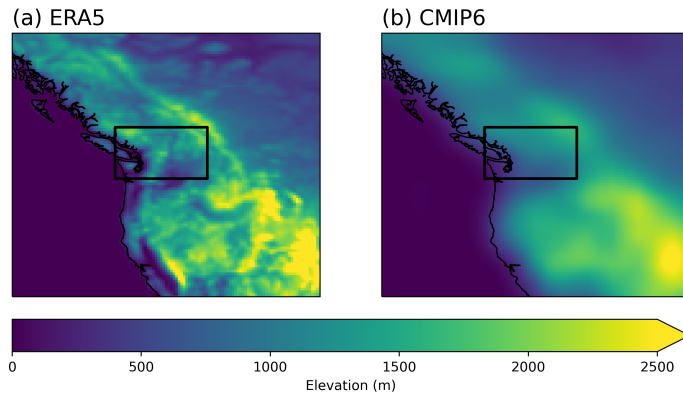
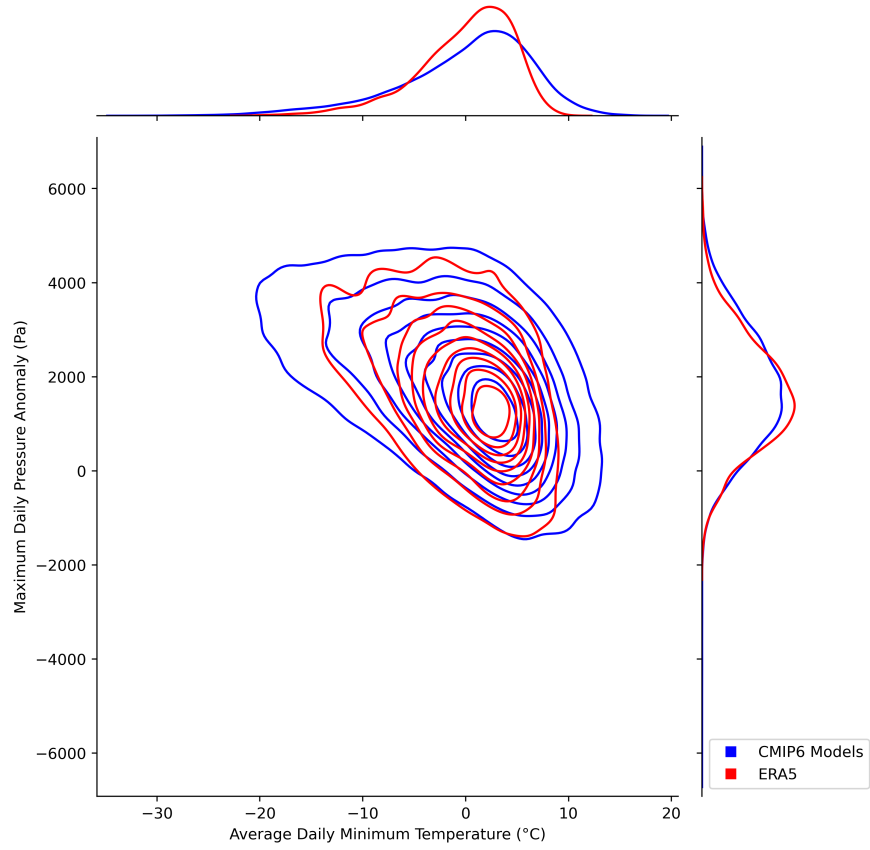
## Abstract

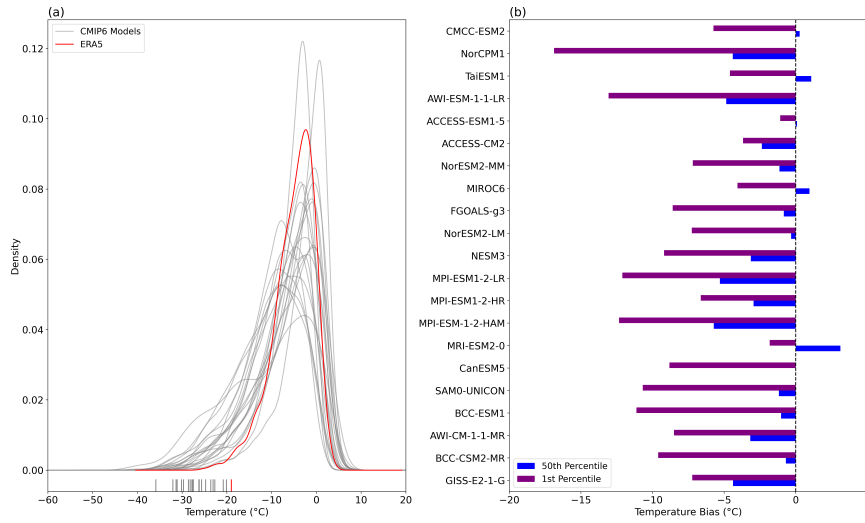
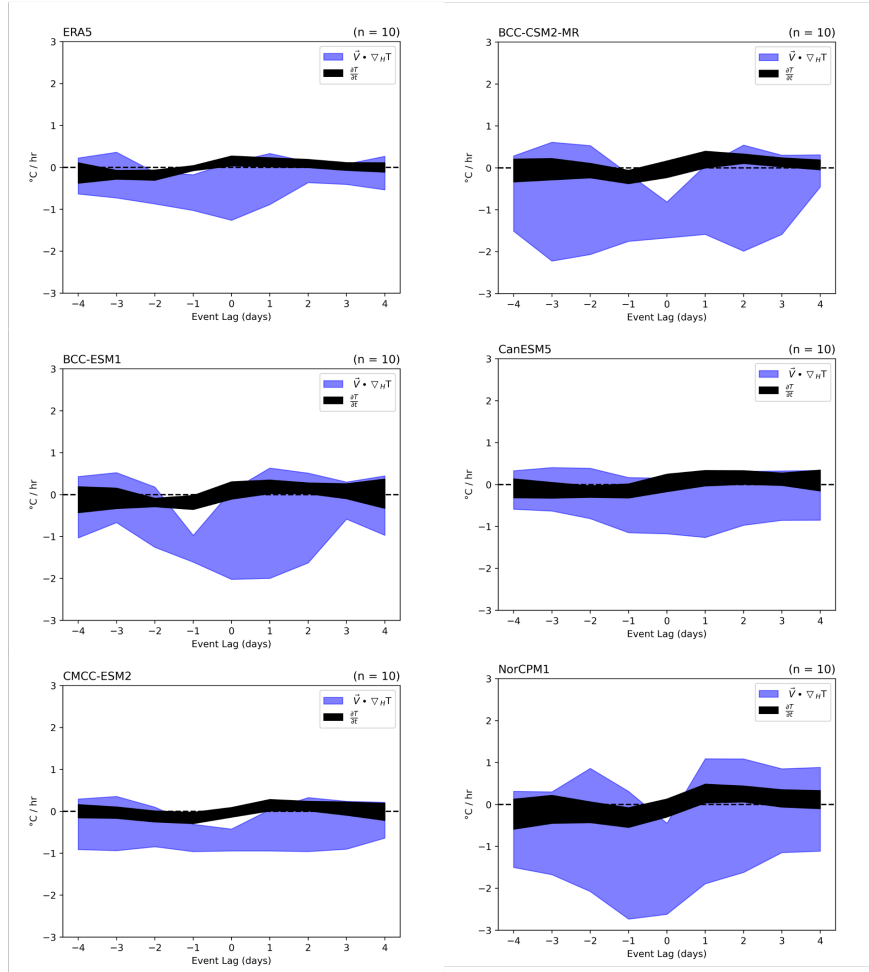
Global climate models often simulate atmospheric conditions incorrectly due to their coarse grid resolution, flaws in their dynamics, and biases resulting from parameterization schemes. Here we document the magnitude and extent of minimum temperature biases in the CMIP6 model ensemble, relative to ERA5. Bias in the southern Cascadia region (i.e. Pacific Northwestern United States and southwestern British Columbia, Canada, spanning from the coast to the Rocky Mountains) stands out relative to the rest of North America, with some models showing a bias in excess of  $-10^{\circ}\text{C}$  in the 1st percentile of daily winter minimum temperature. During the coldest minimum temperature days, the CMIP6 models show an anomalous high in mean sea level pressure in the Northeast Pacific – an atmospheric blocking pattern that is also present in ERA5. While this atmospheric blocking pattern is typically concurrent with cold temperatures across much of North America, terrain barriers such as the Rockies and Cascades prevent the cold air from reaching the Pacific Northwest in observation and reanalysis. Our results suggest that the bias in CMIP6 minimum temperatures is a result of unresolved topography in the Rockies and Cascade mountain ranges, such that the terrain does not adequately block cold air advection from the interior of the continent.











1 **Substantial cold bias during wintertime cold extremes**  
2 **in the southern Cascadia region in historical CMIP6**  
3 **simulations**

4 **Rogers, M.H.<sup>1</sup>, Mauger, G.<sup>1</sup>, Cristea, N.<sup>2</sup>**

5 <sup>1</sup>Climate Impacts Group, University of Washington

6 <sup>2</sup>Department of Civil & Environmental Engineering, University of Washington

7 **Key Points:**

- 8 • CMIP6 models show a pronounced cold bias in the coldest daily minimum tem-  
9 peratures for the Cascadia region of North America.  
10 • In both the ERA5 and CMIP6 models, the coldest temperatures in this region are  
11 associated with atmospheric blocking patterns in the northeast Pacific.  
12 • Due to their poorly resolved topography, CMIP6 models allow excessive advec-  
13 tion of cold continental air during atmospheric blocking events

---

Corresponding author: Matthew Rogers, [rawrgers@uw.edu](mailto:rawrgers@uw.edu)

**Abstract**

Global climate models often simulate atmospheric conditions incorrectly due to their coarse grid resolution, flaws in their dynamics, and biases resulting from parameterization schemes. Here we document the magnitude and extent of minimum temperature biases in the CMIP6 model ensemble, relative to ERA5. Bias in the southern Cascadia region (i.e. Pacific Northwestern United States and southwestern British Columbia, Canada, spanning from the coast to the Rocky Mountains) stands out relative to the rest of North America, with some models showing a bias in excess of  $-10^{\circ}\text{C}$  in the 1st percentile of daily winter minimum temperature. During the coldest minimum temperature days, the CMIP6 models show an anomalous high in mean sea level pressure in the Northeast Pacific – an atmospheric blocking pattern that is also present in ERA5. While this atmospheric blocking pattern is typically concurrent with cold temperatures across much of North America, terrain barriers such as the Rockies and Cascades prevent the cold air from reaching the Pacific Northwest in observation and reanalysis. Our results suggest that the bias in CMIP6 minimum temperatures is a result of unresolved topography in the Rockies and Cascade mountain ranges, such that the terrain does not adequately block cold air advection from the interior of the continent.

**Plain Language Summary**

Global climate models, for a variety of reasons, continue to struggle with recreating some of the observed behaviors of our Earth system. Here, we document one such issue: daily minimum temperatures in western Washington and Southwestern British Columbia that are much colder than we experience. We find that these temperatures occur when extremely cold air is moved from the north into western Washington and southwestern British Columbia. In reality, terrain barriers such as the Rocky and Cascade mountain ranges prevent this air from reaching western Washington and southwestern British Columbia. However, these mountain ranges in the models are much lower and less jagged, which allows the extreme cold temperatures to occur in the models.

**1 Introduction**

Global climate model (GCM) projections of future climate conditions are extensively used in analyses of climate change impacts. GCMs are the primary source of future climate projections, and are the basis for the majority of impact assessments used to inform decision-makers about potential future climate conditions (e.g. Reidmiller et al., 2018). Projected climate change is expected to significantly impact society by affecting necessary aspects such as water availability, human health, and food security Reidmiller et al. (2018). Thus, providing decision-makers with reliable estimates of present and future conditions is crucial for them to make well-informed decisions about future climate-related risks.

Many studies have evaluated GCM performance by using historical simulations as a benchmark to compare to observations and reanalysis data (e.g. Rupp et al., 2013). As a result of such evaluations, GCMs have significantly improved in their simulations of observed atmospheric phenomena in recent years (Edwards, 2011; Sillmann et al., 2013; Flato et al., 2013a). GCMs have shown fidelity in simulating global quantities, and yet continue to have considerable bias on regional scales Flato et al. (2013b) due to a variety of factors, including coarse grid resolution, flaws in their dynamics, and biases resulting from parameterization schemes (Taylor et al., 2012; Knutti & Sedláček, 2013; O’Gorman & Schneider, 2009; Wilcox & Donner, 2007; Wehrli et al., 2018). GCM bias at regional scales presents a barrier for decision-makers in being well-informed on current and future climate conditions. Further assessment of regional GCM bias is important for understanding how reliable GCM simulations are and to what extent they can be utilized.

63 In a preliminary investigation of Coupled Model Intercomparison Project Phase  
 64 5 (CMIP6) models, we found that simulated cold extremes in Puget Sound were often  
 65 below the range of observed temperature extremes. Further analysis of cold extreme events  
 66 in these GCMs showed that the cold biases often affected much of the southern Casca-  
 67 dia region (i.e., Pacific Northwestern United States west of the Rockies along with south-  
 68 western British Columbia, Canada (Fig. 1). The unrealistic nature of minimum temper-  
 69 ature values in these simulations presents a problem for their use in accurately project-  
 70 ing future changes in temperature variability for the Pacific Northwest. Understanding  
 71 when and why these biases occur is imperative for understanding the appropriate uses  
 72 and limitations of minimum temperature data provided by these GCMs.

73 The observed dynamics behind wintertime cold air outbreaks are well-established,  
 74 with many previous studies connecting significant cold-air outbreaks in the United States  
 75 with atmospheric blocking patterns in the Northeast Pacific (e.g. Carrera et al., 2004).  
 76 Atmospheric blocking regimes in the Northeast Pacific, characterized by a persistent an-  
 77 ticyclonic flow anomaly over the gulf of Alaska (Dole, 1986b,a; Higgins & Schubert, 1996;  
 78 Higgins & Mo, 1997), inhibit the eastward progression of synoptic disturbances through  
 79 strong meridional flow. This leads to anomalies in the North Pacific storm tracks (Naka-  
 80 mura & Wallace, 1990) that ultimately advect cold air southward into the United States.  
 81 Carrera et al. (2004) show that average daily temperature anomalies are consistently be-  
 82 low the 10<sup>th</sup> percentile over an area stretching from British Columbia southeastward to  
 83 the central plains of the United States when a North Pacific blocking event occurs. More  
 84 recently, the connections between severe cold conditions during the winter of 2013-14 have  
 85 also been correlated with an atmospheric blocking pattern in the Northeast Pacific Hart-  
 86 mann (2015).

87 For North America specifically, winter stationary wave patterns resulting from orog-  
 88 raphy also have a significant impact on wintertime temperature variability; resulting from  
 89 their influence on horizontal temperature advection Held et al. (2002). Horizontal tem-  
 90 perature advection is known to be the largest contributor to synoptic temperature vari-  
 91 ability in the Northern Hemisphere Lutsko et al. (2019), and previous research suggests  
 92 that terrain plays an important role in how cold air is advected into the United States  
 93 Hartjenstein & Bleck (1991), particularly during atmospheric blocking events in the North-  
 94 east Pacific.

95 Taken together, the known interactions between the atmospheric dynamics and ter-  
 96 rain that lead to cold temperatures in southern Cascadia present two possibilities for the  
 97 existence of the cold temperature bias in the southern Cascadia region. Namely, biases  
 98 in the strength and location of North Pacific atmospheric blocking events leading to stronger  
 99 cold advection into Pacific Northwest North America, and bias in terrain simulation  
 100 in the CMIP6 models that allows cold air to reach areas it normally would not in ob-  
 101 servation. With this, our study has two objectives; (1) to document the magnitude and  
 102 spatial extent of bias in cold minimum temperatures in the southern Cascadia region of  
 103 North America and, (2) to identify when this bias occurs and assess the relative contri-  
 104 butions to this bias from the atmospheric dynamic and terrain bias. Given the localized  
 105 nature of the bias to the southern Cascadia region, we hypothesize that the biases in ex-  
 106 treme daily minimum temperatures in CMIP6 models are related to bias in terrain fea-  
 107 tures allowing cold air to move west of the Rocky and Cascade mountain ranges during  
 108 North Pacific atmospheric blocking events.

## 109 2 Data & Methods

110 We use daily mean sea level pressure, daily minimum temperature data, and grid  
 111 cell elevation data from historical simulations of 13 CMIP6 global climate models (Ta-  
 112 ble 1), obtained using the Pangeo cloud storage platform (<https://pangeo.io>). For val-  
 113 idation, we compare the CMIP6 results to data from the European Centre for Medium-

Model	Citation	Native Resolution
ACCESS-CM2	Dix et al. (2019)	1.25° x 1.875°
ACCESS-ESM1-5	Ziehn et al. (2019)	1.875° x 1.25°
AWI-ESM-1-1-LR	Danek et al. (2020)	1.875° x 1.875°
CanESM5	Swart et al. (2019)	2.8125° x 2.8125°
CMCC-ESM2	Lovato et al. (2021)	0.9375° x 1.25°
MIROC6	Tatebe & Watanabe (2018)	1.40625° x 1.40625°
MPI-ESM1-2-LR	Wieners et al. (2019)	1.875° x 1.875°
MPI-ESM1-2-HR	Jungclaus et al. (2019)	0.9375° x 0.9375°
MRI-ESM2-0	Yukimoto et al. (2019)	2.8125° x 2.8125°
NorCPM1	Bethke et al. (2019)	1.875° x 2.5°
NorESM2-MM	Bentsen et al. (2019)	0.9375° x 1.25°
SAM0-UNICON	Park & Shin (2019)	0.9375° x 1.25°
TaiESM1	Lee & Liang (2019)	0.9375° x 1.25°

114 Range Weather Forecasts Reanalysis version 5 (ERA5) Hersbach et al. (2020), which was  
 115 chosen for its fine default resolution of 0.25° x 0.25° latitude by longitude grid and over-  
 116 all reliability as an accurate reanalysis produce Tarek et al. (2020). All data was regrid-  
 117 ded to a 1°x1° latitude by longitude grid via bilinear interpolation unless otherwise noted,  
 118 and all reported bias for the CMIP6 models is relative to ERA5 data.

119 We evaluate biases in the 1st percentile of daily minimum temperature in order to  
 120 ensure an adequate sample size for the selected time period (1981-2010), though our anal-  
 121 ysis indicates that the results would be the same for a variety of definitions of cold min-  
 122 imum temperatures. Hereafter we refer to values below the 1st percentile threshold as  
 123 “extreme cold”.

### 124 3 Results

125 Our results are divided into two sections. The first section focuses on the documen-  
 126 tation of extreme minimum temperature bias, its spatial extent and how pervasive it is  
 127 across CMIP6 models. The second section investigates the source of wintertime extreme  
 128 minimum temperature bias in the southern Cascadia region in CMIP6 models.

#### 129 3.1 Bias Documentation

130 Preliminary findings have shown isolated events with minimum temperatures well  
 131 below observed values in the Puget Sound region; however, the extent and magnitude  
 132 of this bias has yet to be assessed. Fig. 1a shows the bias in the multi-model mean 1st  
 133 percentile minimum DJF temperature (1981-2010) for CMIP6 models relative to ERA5  
 134 for North America. The bias in the southern Cascadia region extending southeast into  
 135 the mountain west region stands out relative to the rest of North America, excluding per-  
 136 haps the southern coast of Alaska. The magnitude of the extreme minimum tempera-  
 137 ture bias for several grid cells within this region shows an ensemble average bias exceed-  
 138 ing -5°C, which is a stark departure from observed values. Fig. 1b shows that the sign  
 139 of the bias is the same for all CMIP6 models analyzed, without exception. These results  
 140 suggest two things: (1) CMIP6 models have a systematic problem in simulating realis-  
 141 tic extreme cold air in the southern Cascadia region; and (2) the source of this bias is  
 142 likely specific to this region, given that biases in other regions are not as large, are not  
 143 necessarily of the same sign, and show less consistency among models. Hereafter, our anal-  
 144 ysis will be focused on this region, though we note that there are other regions with sim-  
 145 ilar bias characteristics (e.g., southeastern Alaska). We select a sub-region that isolates

146 the largest magnitude and agreement in the sign of bias in the CMIP6 ensemble (Fig.  
147 1a, b: 46.5N - 51.5N, 125W - 116W).

148 Our first goal is to determine whether the bias in the minimum temperature is unique  
149 to the coldest temperatures or is present throughout the entire distribution of winter-  
150 time minimum temperatures. Fig. 2a compares the probability distributions of daily win-  
151 tertime minimum temperatures (1981-2010) averaged over the southern Cascadia region  
152 for ERA5 and the CMIP6 models. The daily minimum temperature distributions for most  
153 models shown in Fig. 2a are more left skewed relative to ERA5, meaning that CMIP6  
154 models in this region consistently simulate colder minimum temperatures than in the ob-  
155 servations. This does not appear to be a result of a shifted distribution, since the right  
156 tail of the distributions are similar. Instead, the bias appears to be confined to the lower  
157 end of the minimum temperature distributions in ERA5 and CMIP6 models. The cold  
158 bias is consistently present across a range of the lower quantiles in the distribution, but  
159 begins to be less consistently negative around the XXth percentile.

160 To better visualize how the bias in 1st percentile minimum temperatures compares  
161 to bias in the median, Fig. 2b shows the bias in 50th percentile and 1st percentile daily  
162 minimum wintertime temperatures for each model in this study, averaged over the suth-  
163 ern Cascadia region. Consistently across the ensemble, the bias in the 1st percentile min-  
164 imum temperatures far exceeds the bias in the median for the southern Cascadia region,  
165 again suggesting that the distributions for minimum temperature in CMIP6 models for  
166 the southern Cascadia region are skewed left relative to ERA5. Notably, the absolute  
167 magnitude of the 1st percentile bias for many models exceeds  $-10^{\circ}\text{C}$ . The results show  
168 highly skewed probability distributions (Fig. 2a) and a larger magnitude of bias in the  
169 1st percentiles relative to the median relative to ERA5, suggesting that the bias in ex-  
170 treme minimum temperatures is uncoupled from systematic bias in the minimum tem-  
171 perature distributions.

172 We have shown that a large bias in minimum temperature extremes for the CMIP6  
173 models is isolated to the southern Cascadia region (Fig. 1). We have also demonstrated  
174 that this bias in minimum temperatures is unique to the cold extremes (Fig. 2). Next,  
175 we investigate potential sources for this minimum temperature bias

### 176 3.2 Sources of Cold Minimum Temperature Bias

177 Informed by previous research focused on cold temperatures in North America, we  
178 hone in on two potential contributors to the cold minimum temperature bias in south-  
179 ern Cascadia in the CMIP6 models: (1) biases in the strength and location of North Pa-  
180 cific atmospheric blocking events, and (2) bias in terrain simulation in the CMIP6 mod-  
181 els. We begin this section by analyzing (1).

182 To investigate the role of cold air advection in the southern Cascadia extreme min-  
183 imum temperature bias we start by identifying the associated synoptic weather patterns  
184 in the models and reanalysis. Fig. 3 shows a composite of mean sea level pressure (MSLP)  
185 anomalies relative to DJF average (1981-2010) during days with minimum temperature  
186 below the 1st percentile. Results for both ERA5 and the CMIP6 multi-model mean show  
187 large areas of positive MSLP anomalies over Alaska and the Gulf of Alaska, which is con-  
188 sistent with the Northeast Pacific atmospheric blocking pattern we would expect dur-  
189 ing the coldest temperatures over much of North America. The CMIP6 multi-model mean  
190 shows anomaly magnitudes less than ERA5, but, upon further investigation, this is a re-  
191 sult of the CMIP6 models simulating slightly different positions of the block and not a  
192 result of a deficiency in simulated anomaly magnitude. The similarities between the anomaly  
193 patterns in Fig. 3 indicates that the CMIP6 models capture the synoptic MSLP anomaly  
194 pattern associated with the coldest minimum temperatures in the southern Cascadia re-  
195 gion. The similar patterns suggest that the associated synoptic-scale conditions are sim-  
196 ulated accurately by the CMIP6 models. Thus, we infer that the primary cause of the

197 bias is not the synoptic-scale weather patterns but how they manifest conditions at the  
198 surface.

199 To further investigate whether synoptic patterns during the coldest days in the south-  
200 ern Cascadia region in ERA5 and the CMIP6 models are similar, we compare MSLP anoma-  
201 lies over Alaska against minimum daily temperatures in the southern Cascadia region  
202 (Fig. 4). MSLP anomalies are averaged over an area encompassing the largest anoma-  
203 lies, as outlined in Fig. 3. The range of pressure anomalies in CMIP6 models is much  
204 more consistent with the range in ERA5, though the largest anomalies are slightly higher  
205 than in ERA5 and the mode of the distribution is lower. In contrast, the minimum tem-  
206 perature anomalies have very different distributions. In particular, the lowest temper-  
207 atures in the CMIP6 models are up to 10°C colder than in ERA5, primarily occurring  
208 when the maximum SLP anomalies over Alaska are large. Taken together, the similar-  
209 ities in SLP magnitudes (Fig. 4) and patterns (Fig. 3) in the CMIP6 models and ERA5,  
210 along with the differences in minimum temperature anomalies, suggest that incorrect sim-  
211 ulation of dynamics is not the primary cause of the minimum temperature bias. If in-  
212 correct simulation of underlying dynamics of cold minimum temperatures were the cause  
213 of this bias, we would expect to see considerable differences in the SLP anomaly pattern  
214 or magnitude, or both.

215 Since the minimum temperature biases are large (some exceeding -10°C, Fig. 2)  
216 despite no major biases in dynamics, we have hypothesized that how temperature ad-  
217 vection manifests at the surface plays the main role in driving the bias. A previous eval-  
218 uation of land surface energy fluxes in the CMIP6 models do not identify the southern  
219 Cascadia region as having significant bias in sensible, latent, or ground heat flux Li et  
220 al. (2021), again suggesting that cold air advection is the primary explanation for the  
221 extreme minimum temperature bias. To examine this more closely, we estimate the hourly  
222 contributions of the diabatic and adiabatic terms of the temperature tendency formula  
223 Holton & Hakim (2013) to identify relative contributions to temperature change lead-  
224 ing up to the 10 coldest minimum temperature days (SI 1). Of the select GCMs, all five  
225 models (BCC-CSM2-MR, BCC-ESM1, CanESM5, CMCC-ESM1, NorCPM1) analyzed  
226 indicate that the primary driver of cold temperatures is cold air advection. Further, some  
227 of the GCMs indicate minimum values of temperature advection upwards of -2°C/hr, which  
228 is considerably more than shown in ERA5. Taken together, the synoptic MSLP patterns  
229 (Fig. 3), the distribution of pressure anomalies versus minimum temperatures (Fig. 4),  
230 and the contribution of temperature advection to temperature change in the southern  
231 Cascadia region (SI 1), all of the evidence suggests that anomalous cold air advection  
232 is the primary cause of the extreme minimum temperature bias in CMIP6 models. Thus,  
233 we shift our focus to potential contributor (2), bias in terrain simulation in the CMIP6  
234 models.

235 Topographic barriers play a large role in the spatial distribution of cold temper-  
236 atures during cold air outbreaks. This means that some bias in extreme minimum tem-  
237 peratures is likely associated with the coarse resolution of CMIP6 models and the result-  
238 ing inadequacy in resolving the elevation profile of the southern Cascadia region. Fig.  
239 5 shows the terrain elevation for western North America for ERA5 and CMIP6. Sim-  
240 ilar to the results from (Mahony et al., 2021), the terrain in the CMIP6 models is much  
241 smoother and generally lower in elevation than the terrain in ERA5 (Fig. 5b), especially  
242 in Western Washington and the Rockies just northeast of Vancouver Island. The Cas-  
243 cade Range, for example, is essentially missing in the models, while the Rockies are more  
244 broad, with a crest that is several hundred meters below the maximum in ERA5.

245 An elevation cross section through the southern Cascadia region extending into cen-  
246 tral Canada (Fig. 6; black shading) illustrates the stark difference in the elevation pro-  
247 files for the CMIP6 models (multi-model mean) and ERA5. The Cascade and Olympic  
248 mountain ranges are absent from the CMIP6 elevation profile, and, as shown in Fig. 5,  
249 the apex of the Rocky mountains is considerably lower than in ERA5. When overlaid

with the average potential temperature during the coldest percentile in minimum temperature days (Fig. 6; black lines) we see that the west-east potential temperature gradient is relatively small, whereas in ERA5 the gradient between the west and east side of the Cascades and Rocky mountains is large. Furthermore, if we neglect diabatic effects then potential temperature is conserved and can be considered a tracer for air masses as they are advected. Taking this angle, we focus on the 260K potential temperature contour in Fig. 6. In ERA5, this contour is confined to the east of the Rockies and Cascades, while in the CMIP6 models this contour extends all the way to the coast. This suggests that the cold air mass with potential temperature of 260K, when advected into the region, was able to advect over the terrain to the coast of the southern Cascadia region in the CMIP6 models, whereas in ERA5 the cold air was unable to be advected to the coast.

## 4 Discussion & Conclusions

This study identified bias in extreme minimum temperatures in the southern Cascadia region of North America in the CMIP6 models, which we showed were a likely result of unresolved terrain features. Our results suggest the bias is unique to the region given the high level of agreement and magnitude of the bias in 1st percentile wintertime daily minimum temperatures (Fig. 1). We also showed that the median bias is not consistent with the bias in extreme minimum temperatures for all models, indicating that the bias is due to a misrepresentation of the mechanisms affecting the coldest events in this region.

Prior research on synoptic weather patterns has shown that cold temperatures across North America are associated with atmospheric blocking patterns in the Northeast Pacific. We confirm that both the ERA5 and CMIP6 models show synoptic MSLP patterns that are consistent with this finding (Fig. 3). Additional analysis shows that the MSLP distributions for CMIP6 are similar to those for ERA5 over Alaska and the northeast Pacific (Fig. 4). While the magnitudes of the MSLP anomalies in Alaska are similar in ERA5 and the CMIP6 models, the coldest minimum temperatures in the southern Cascadia region are considerably colder in CMIP6 models relative to ERA5. The highly localized nature of the bias, the demonstrated association with atmospheric blocking in the Northeast Pacific (Figs. 3, 4), and the relative absence of diabatic influences on temperatures during these events all point to errors in simulating cold air advection across the Cascade and Rocky mountain ranges. This is consistent with previous studies showing the importance of terrain in influencing how cold air is advected into North America during atmospheric blocking events in the Northeast Pacific.

The CMIP6 multi-model mean orography showed that models under-resolve the Cascade and Rocky mountains. A horizontal cross section across this domain confirmed that GCM topography differs substantially from actual elevations. Potential temperature contours composited over the coldest minimum temperature days showed the coldest air being confined to the east of the Rockies in ERA5. The same cross section in CMIP6 shows that this cold air mass is much less restricted due to inadequate representation of the terrain barriers, resulting in a significantly diminished temperature contrast between the maritime vs continental sides of each range. Taken together, the results again suggest that adequate resolution of the terrain is needed to accurately simulate extreme minimum temperatures in the southern Cascadia region of North America.

There are several limitations to this study. The number of models used in this study was limited to 13, with only 3 having the hourly temperature and wind data needed to estimate temperature advection during extreme minimum temperature events. In order to make a generalized statement about all CMIP6 models, and confidently rule out potential contributions from diabatic heating, more CMIP6 results would need to be analyzed.

301 Further, this study did not consider the role of ocean-atmosphere interactions on  
302 cold minimum temperatures, which are likely to exhibit a controlling factor on temper-  
303 ature variations in the southern Cascadia region. While latent and sensible heat fluxes  
304 contribute to the diabatic term of the temperature tendency formula (SI XXX), the lack  
305 of hourly data for the CMIP6 models limits our analysis of how this contributes to ex-  
306 treme minimum temperatures in the southern Cascadia region. It is likely, however, that  
307 given the coarse resolution of the CMIP6 models, heat fluxes from complex bays such  
308 as Puget Sound are under-represented. Indeed, Fig. 6 appears to show warmer poten-  
309 tial temperatures west of the Cascade mountain range in ERA5 compared to the CMIP6  
310 models, which may be evidence of Puget Sound’s moderating influence. Although the  
311 evidence suggests that cold air advection is a primary driver of extreme wintertime min-  
312 imum temperature bias in the CMIP6 models, a secondary explanation could be related  
313 to CMIP6 model representation of marine air influence in the southern Cascadia region.  
314 This may be one reason the cold biases are greater west of the Cascades than they are  
315 between the Cascades and the Rockies. Future work could use GCM surface fluxes to  
316 estimate the relative contributions of diabatic heating relative to cold advection.

317 Resources for assessing future climate change are largely limited to the climate change  
318 simulations produced for the Coupled Model Intercomparison Projects. In order to plan  
319 for climate change impacts it is particularly important to identify and address GCM bi-  
320 ases. Strategies to address the extreme minimum temperature bias could include finer  
321 resolution GCM simulations, dynamical downscaling over a domain that encompasses  
322 all relevant topography, and analyses of historical events to understand the relationships  
323 between large-scale conditions and extreme minimum temperatures in the southern Cas-  
324 cadia region. To better elucidate the causes of this bias, future GCM simulations should  
325 include the hourly fields needed to estimate the temperature tendency: At a minimum,  
326 hourly wind and temperature data, and ideally also latent, sensible, and radiative fluxes  
327 at the surface. Finer spatial scales may eliminate the issue of the cold minimum tem-  
328 perature bias altogether if it captures terrain features in Cascadia sufficiently.

329 Alternatively, statistically or dynamically downscaling could be designed to bet-  
330 ter capture extreme minimum temperatures. In order to address the issue, downscaling  
331 approaches would need to be designed so as not to erroneously pass along biases from  
332 the input GCM data. For the minimum temperature bias documented here, the bias  
333 for southern Cascadia was originally discovered in dynamically downscaled CMIP5 data.  
334 In the case of these simulations, the domain of the downscaling covered the US Pacific  
335 Northwest, but did not extend far enough north to capture the topography of the Cana-  
336 dian Cascades and Rockies, and therefore could not correct for the anomalous cold ad-  
337 vection through this topography in the GCMs.

338 In the meantime, communities needing to plan for changes in extreme cold condi-  
339 tions are limited by a lack of suitable GCM or downscaled projections. In areas where  
340 the extreme minimum temperature bias is present, stakeholders should consider alter-  
341 native approaches to assessing impacts. Alternatives could include sensitivity testing in  
342 order to identify thresholds for impact, assuming that extreme minimum temperatures  
343 warm at the same rate as the annual or seasonal average temperature, or assessing trends  
344 from observations. While GCMs remain the primary information resource for prepar-  
345 ing for climate change, these alternatives can provide decision-makers with important  
346 information to help them prepare for the impacts of climate change.

## 347 5 Open Research

348 CMIP6 data used in this study was accessed using the Pangeo cloud catalog (<https://pangeo.io>)  
349 (Abernathy et al., 2017), and ERA5 data is available for download from the Coperni-  
350 cus climate data store (<https://cds.climate.copernicus.eu>) (Hersbach et al., 2020). Fig-  
351 ures in this study were created with Matplotlib version 3.4.3, available at <https://matplotlib.org/>.

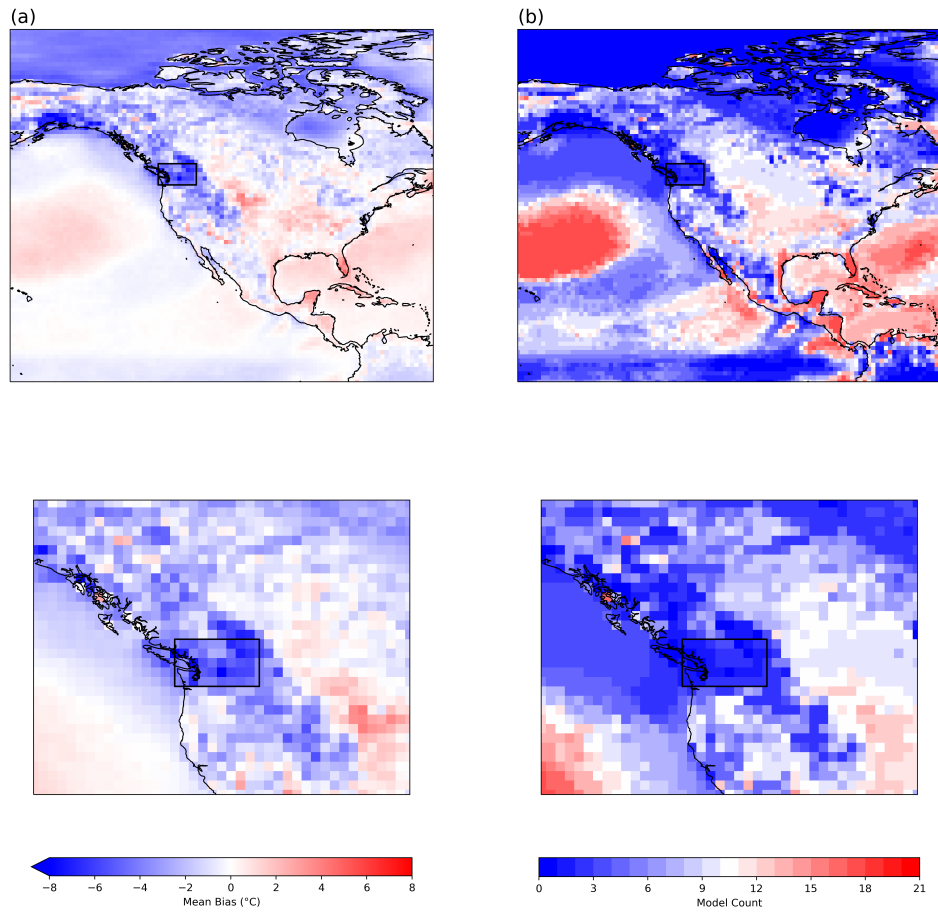


**Figure 1.** (column a) multi-model mean bias in 1st percentile daily minimum winter (DJF) temperature (1981-2010) for 13 CMIP6 models relative to ERA5, and (column b) model agreement on positive sign of bias. The black boxes denote the area of interest for this study (46.5°N-51.5°N,125°W-116°W)

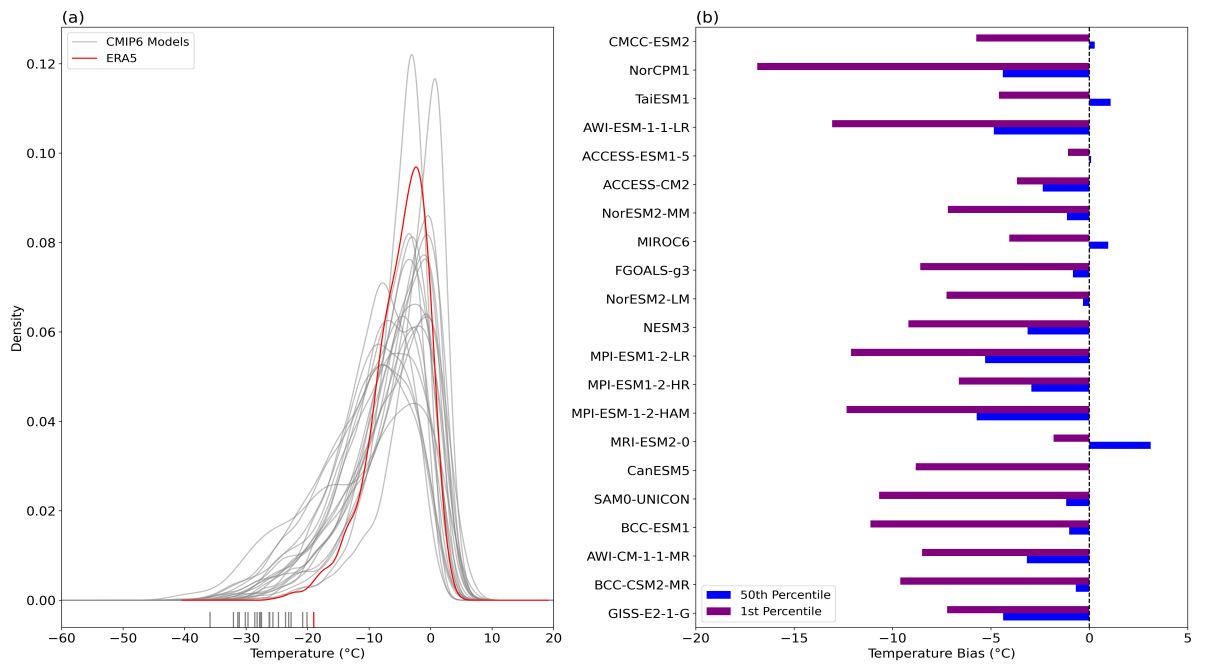


**Figure 2.** (a) Probability density functions (PDFs) of DJF daily minimum temperatures (°C) averaged over the domain 46.5N - 51.5N and 125W - 116W for 13 CMIP6 models (gray) and ERA5 (red) from 1981-2010, and (b) individual CMIP6 model bias in the 1st (purple) and 50th (blue) percentile daily minimum temperature (°C) over the same domain and time period as (a).

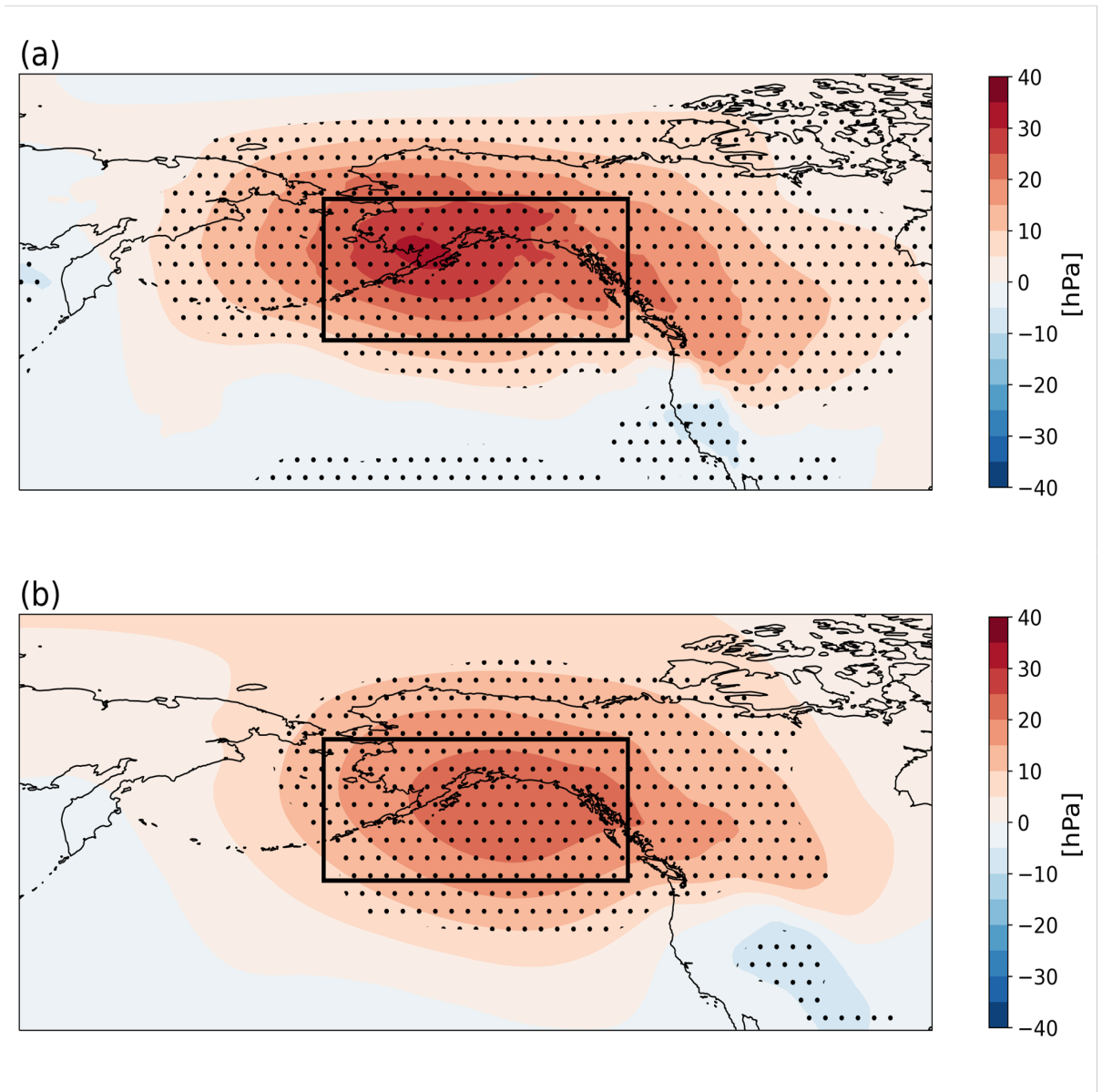


**Figure 3.** (a) Composite mean sea level pressure anomalies (MSLP; hPa) during days when the average minimum temperature in the PNW region is below the 1st percentile for ERA5, and (b) multi-model mean composite MSLP anomalies during days when the average minimum temperature in the PNW region is below the 1st percentile for the CMIP6 models. Black stippling indicates statistical significance at the 95% confidence level using a bootstrapping method with 1000 iterations. Black box indicates the region of interest for investigating MSLP anomalies is the next analysis.

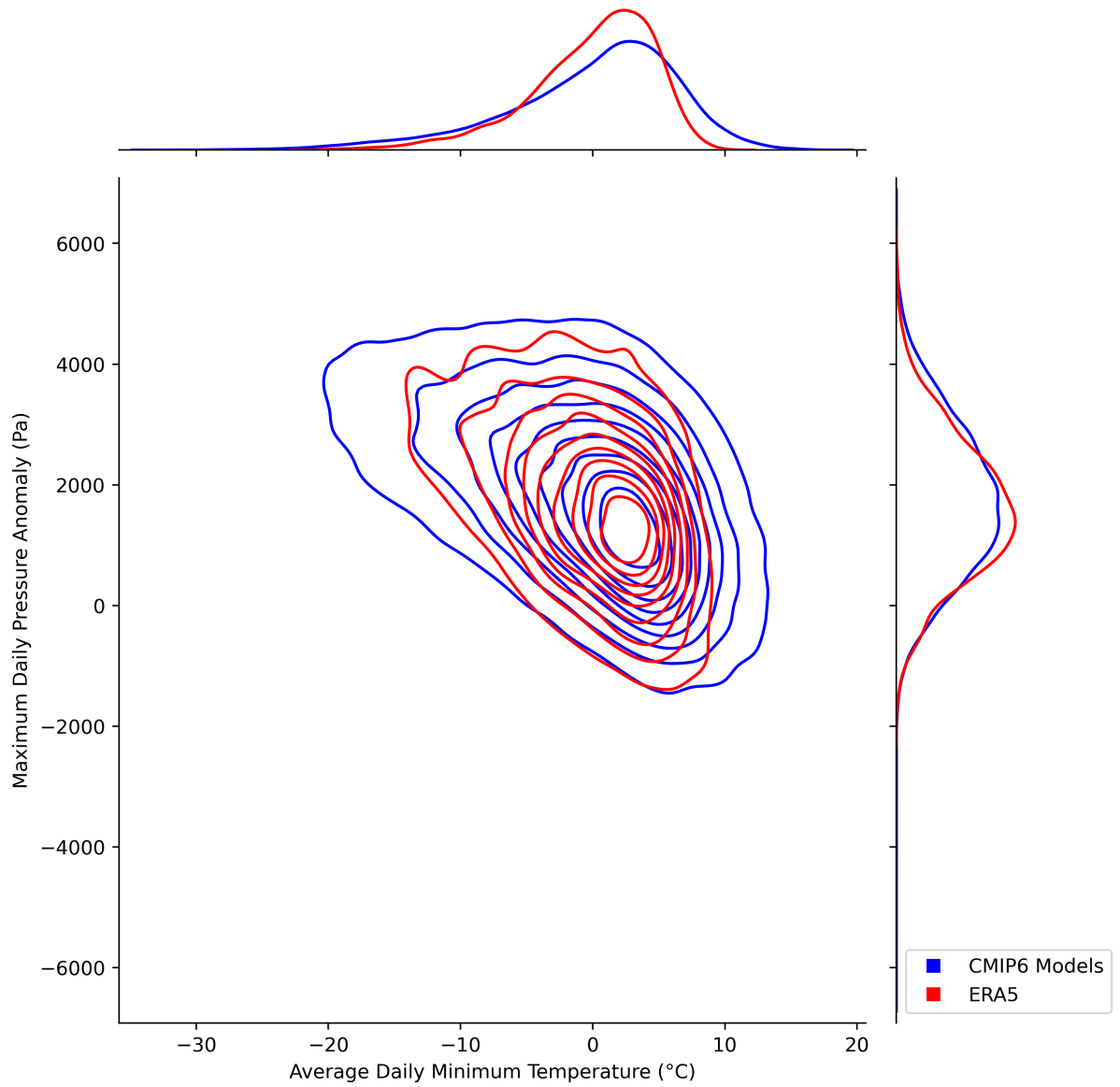


**Figure 4.** Density plot of daily minimum temperature averaged over the southern Cascadia region ((46.5°N-51.5°N,125°W-116°W)) vs. the minimum daily MSLP anomalies over the Gulf of Alaska (48°N-67°N,190°W-230°W) for the days below the 1st percentile minimum daily temperature in the southern cascadia region. ERA5 data is in red and the 13 CMIP6 models are in blue. External probability functions are shown for daily minimum temperatures (x-axis; top) and minimum dails MSLP anomalies (y-axis; top).

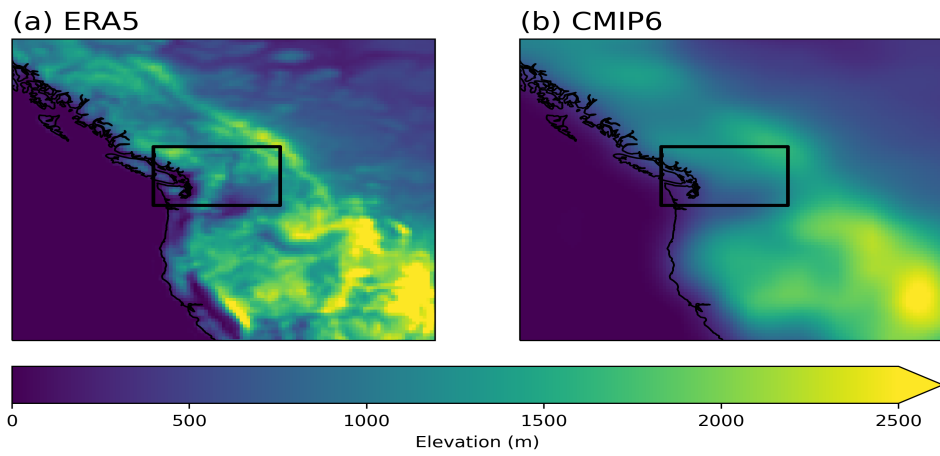


**Figure 5.** Elevation of grid cells in (a) ERA5 and (b) CMIP6 multi-model mean. CMIP6 grids were interpolated to the ERA5 grid ( $0.25^\circ$  latitude  $\times$   $0.25^\circ$  longitude) using bilinear interpolation. Area outlined by the black box in each subplot ( $46.5^\circ\text{N}$ - $51.5^\circ\text{N}$ ,  $125^\circ\text{W}$ - $116^\circ\text{W}$ ) is the southern Cascadia region, or the selected high-bias-high-agreement area.

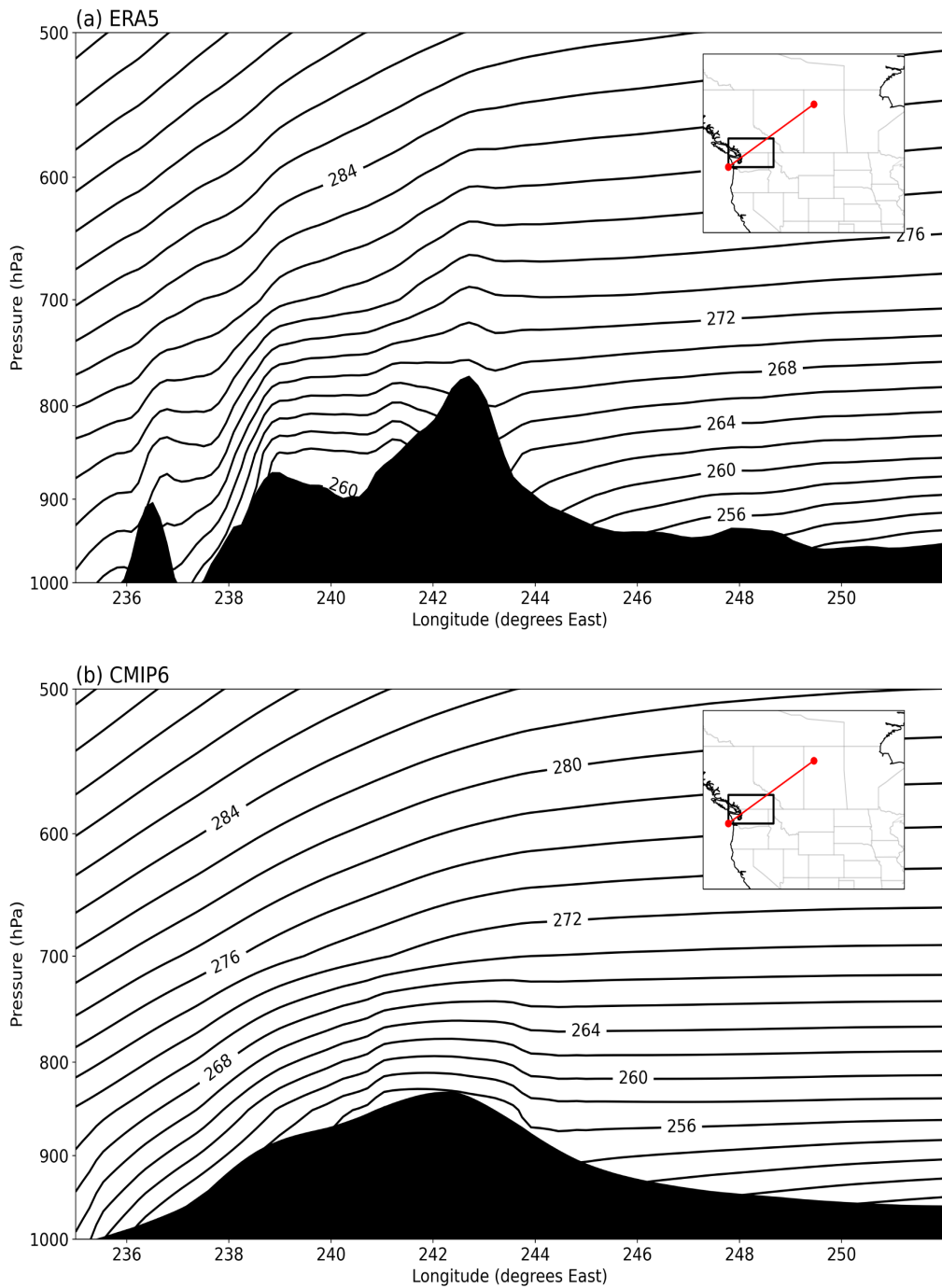


**Figure 6.** Vertical cross-section (red line) of mean potential temperature (contours) for days below the 1st percentile in spatially-averaged DJF minimum temperature for the area bounded by 46.5°N-51.5°N and 125°W-116°W (black box) for (a) ERA5 and (b) CMIP6 multi-model mean.

## References

- 352 Abernathy, R., Kevin Paul, Joe Hamman, Matthew Rocklin, Chiara Lepore, Michael  
353 Tippett, ... Vento, D. D. (2017, 8). *Pangeo NSF Earthcube proposal*. Re-  
354 trieved from [https://figshare.com/articles/journal\\_contribution/  
355 Pangeo\\_NSF\\_Earthcube\\_Proposal/5361094](https://figshare.com/articles/journal_contribution/Pangeo_NSF_Earthcube_Proposal/5361094) doi: 10.6084/m9.figshare.5361094.v1
- 357 Bentsen, M., Olivière, D. J. L., Seland, Y., Toniazzo, T., Gjermundsen, A., Graff, L. S.,  
358 ... Schulz, M. (2019). *Ncc noresm2-mm model output prepared for cmip6 cmip*.  
359 Earth System Grid Federation. Retrieved from [https://doi.org/10.22033/  
360 ESGF/CMIP6.506](https://doi.org/10.22033/ESGF/CMIP6.506) doi: 10.22033/ESGF/CMIP6.506
- 361 Bethke, I., Wang, Y., Counillon, F., Kimmritz, M., Fransner, F., Samuelson, A., ...  
362 Keenlyside, N. (2019). *Ncc norcpm1 model output prepared for cmip6 cmip*. Earth  
363 System Grid Federation. Retrieved from [https://doi.org/10.22033/ESGF/  
364 CMIP6.10843](https://doi.org/10.22033/ESGF/CMIP6.10843) doi: 10.22033/ESGF/CMIP6.10843
- 365 Carrera, M. L., Higgins, R. W., & Kousky, V. E. (2004, December). Downstream  
366 Weather Impacts Associated with Atmospheric Blocking over the Northeast  
367 Pacific. *Journal of Climate*, 17(24), 4823–4839. Retrieved 2021-08-04, from  
368 <https://journals.ametsoc.org/view/journals/clim/17/24/jcli-3237.1.xml>  
369 doi: 10.1175/JCLI-3237.1
- 370 Danek, C., Shi, X., Stepanek, C., Yang, H., Barbi, D., Hegewald, J., & Lohmann, G.  
371 (2020). *Awi awi-esm1.1lr model output prepared for cmip6 cmip*. Earth System  
372 Grid Federation. Retrieved from <https://doi.org/10.22033/ESGF/CMIP6.9301>  
373 doi: 10.22033/ESGF/CMIP6.9301
- 374 Dix, M., Bi, D., Dobrohotoff, P., Fiedler, R., Harman, I., Law, R., ... Yang, R.  
375 (2019). *Csiro-arccss access-cm2 model output prepared for cmip6 cmip*. Earth  
376 System Grid Federation. Retrieved from [https://doi.org/10.22033/ESGF/  
377 CMIP6.2281](https://doi.org/10.22033/ESGF/CMIP6.2281) doi: 10.22033/ESGF/CMIP6.2281
- 378 Dole, R. M. (1986a). The life cycles of persistent anomalies and blocking over the  
379 north pacific. In B. Saltzman, R. Benzi, & A. C. Wiin-Nielsen (Eds.), *Anoma-  
380 lous atmospheric flows and blocking* (Vol. 29, p. 31-69). Elsevier. Retrieved from  
381 <https://www.sciencedirect.com/science/article/pii/S0065268708600345>  
382 doi: [https://doi.org/10.1016/S0065-2687\(08\)60034-5](https://doi.org/10.1016/S0065-2687(08)60034-5)
- 383 Dole, R. M. (1986b). Persistent anomalies of the extratropical northern hemi-  
384 sphere wintertime circulation: Structure. *Monthly Weather Review*, 114(1),  
385 178 - 207. Retrieved from [https://journals.ametsoc.org/view/journals/  
386 mwre/114/1/1520-0493\\_1986\\_114\\_0178\\_paoten\\_2\\_0\\_co\\_2.xml](https://journals.ametsoc.org/view/journals/mwre/114/1/1520-0493_1986_114_0178_paoten_2_0_co_2.xml) doi: 10.1175/  
387 1520-0493(1986)114(0178:PAOTEN)2.0.CO;2
- 388 Edwards, P. N. (2011). History of climate modeling. *WIREs Climate Change*, 2(1),  
389 128-139. Retrieved from [https://wires.onlinelibrary.wiley.com/doi/abs/10  
390 .1002/wcc.95](https://wires.onlinelibrary.wiley.com/doi/abs/10.1002/wcc.95) doi: <https://doi.org/10.1002/wcc.95>
- 391 Flato, G., Marotzke, J., Abiodun, B., Braconnot, P., Chou, S., Collins, W., ...  
392 Rummukainen, M. (2013b). Climate change 2013: The physical science basis.  
393 contribution of working group I to the fifth assessment report of the intergovern-  
394 mental panel on climate change. In T. Stocker et al. (Eds.), (chap. Evaluation  
395 of Climate Models). Cambridge, United Kingdom and New York, NY, USA:  
396 Cambridge University Press.
- 397 Flato, G., Marotzke, J., Abiodun, B., Braconnot, P., Chou, S. C., Collins, W., ...  
398 Rummukainen, M. (2013a). Climate change 2013: The physical science basis.  
399 contribution of working group I to the fifth assessment report of the intergovern-  
400 mental panel on climate change. In T. F. Stocker et al. (Eds.), (pp. 741–882).  
401 Cambridge, UK: Cambridge University Press.
- 402 Hartjenstein, G., & Bleck, R. (1991). Factors affecting cold-air outbreaks east of  
403 the rocky mountains. *Monthly Weather Review*, 119(9), 2280 - 2292. Retrieved  
404 from [https://journals.ametsoc.org/view/journals/mwre/119/9/1520-0493  
405 \\_1991\\_119\\_2280\\_facaoe\\_2\\_0\\_co\\_2.xml](https://journals.ametsoc.org/view/journals/mwre/119/9/1520-0493_1991_119_2280_facaoe_2_0_co_2.xml) doi: 10.1175/1520-0493(1991)119(2280:

- 406 FACAOE)2.0.CO;2
- 407 Hartmann, D. L. (2015). Pacific sea surface temperature and the winter of 2014.  
 408 *Geophysical Research Letters*, *42*(6), 1894-1902. Retrieved from [https://agupubs](https://agupubs.onlinelibrary.wiley.com/doi/abs/10.1002/2015GL063083)  
 409 [.onlinelibrary.wiley.com/doi/abs/10.1002/2015GL063083](https://agupubs.onlinelibrary.wiley.com/doi/abs/10.1002/2015GL063083) doi: [https://doi](https://doi.org/10.1002/2015GL063083)  
 410 [.org/10.1002/2015GL063083](https://doi.org/10.1002/2015GL063083)
- 411 Held, I. M., Ting, M., & Wang, H. (2002, August). Northern Winter Sta-  
 412 tionary Waves: Theory and Modeling. *Journal of Climate*, *15*(16), 2125–  
 413 2144. Retrieved 2021-10-29, from [https://journals.ametsoc.org/view/](https://journals.ametsoc.org/view/journals/clim/15/16/1520-0442_2002_015_2125_nswsta_2.0.co_2.xml)  
 414 [journals/clim/15/16/1520-0442\\_2002\\_015\\_2125\\_nswsta\\_2.0.co\\_2.xml](https://journals.ametsoc.org/view/journals/clim/15/16/1520-0442_2002_015_2125_nswsta_2.0.co_2.xml) doi:  
 415 [10.1175/1520-0442\(2002\)015\(2125:NWSWTA\)2.0.CO;2](https://doi.org/10.1175/1520-0442(2002)015(2125:NWSWTA)2.0.CO;2)
- 416 Hersbach, H., Bell, B., Berrisford, P., Hirahara, S., Horányi, A., Muñoz-Sabater,  
 417 J., ... Thépaut, J.-N. (2020). The era5 global reanalysis. *Quarterly Jour-*  
 418 *nal of the Royal Meteorological Society*, *146*(730), 1999-2049. Retrieved from  
 419 <https://rmets.onlinelibrary.wiley.com/doi/abs/10.1002/qj.3803> doi:  
 420 <https://doi.org/10.1002/qj.3803>
- 421 Higgins, R. W., & Mo, K. C. (1997). Persistent north pacific circulation  
 422 anomalies and the tropical intraseasonal oscillation. *Journal of Climate*,  
 423 *10*(2), 223 - 244. Retrieved from [https://journals.ametsoc.org/view/](https://journals.ametsoc.org/view/journals/clim/10/2/1520-0442_1997_010_0223_pnpcaa_2.0.co_2.xml)  
 424 [journals/clim/10/2/1520-0442\\_1997\\_010\\_0223\\_pnpcaa\\_2.0.co\\_2.xml](https://journals.ametsoc.org/view/journals/clim/10/2/1520-0442_1997_010_0223_pnpcaa_2.0.co_2.xml) doi:  
 425 [10.1175/1520-0442\(1997\)010\(0223:PNPCAA\)2.0.CO;2](https://doi.org/10.1175/1520-0442(1997)010(0223:PNPCAA)2.0.CO;2)
- 426 Higgins, R. W., & Schubert, S. D. (1996). Simulations of persistent north pacific cir-  
 427 culation anomalies and interhemispheric teleconnections. *Journal of Atmospheric*  
 428 *Sciences*, *53*(1), 188 - 207. Retrieved from [https://journals.ametsoc.org/](https://journals.ametsoc.org/view/journals/atsc/53/1/1520-0469_1996_053_0188_sopnpc_2_0_co_2.xml)  
 429 [view/journals/atsc/53/1/1520-0469\\_1996\\_053\\_0188\\_sopnpc\\_2\\_0\\_co\\_2.xml](https://journals.ametsoc.org/view/journals/atsc/53/1/1520-0469_1996_053_0188_sopnpc_2_0_co_2.xml)  
 430 doi: [10.1175/1520-0469\(1996\)053\(0188:SOPNPC\)2.0.CO;2](https://doi.org/10.1175/1520-0469(1996)053(0188:SOPNPC)2.0.CO;2)
- 431 Holton, J., & Hakim, G. (2013). *An introduction to dynamic meteorology*. Academic  
 432 Press, Cambridge. doi: <https://doi.org/10.1016/C2009-0-63394-8>
- 433 Jungclaus, J., Bittner, M., Wieners, K.-H., Wachsmann, F., Schupfner, M.,  
 434 Legutke, S., ... Roeckner, E. (2019). *Mpi-m mpiesm1.2-hr model output*  
 435 *prepared for cmip6 cmip*. Earth System Grid Federation. Retrieved from  
 436 <https://doi.org/10.22033/ESGF/CMIP6.741> doi: [10.22033/ESGF/CMIP6.741](https://doi.org/10.22033/ESGF/CMIP6.741)
- 437 Knutti, R., & Sedláček, J. (2013, April). Robustness and uncertainties in  
 438 the new CMIP5 climate model projections. *Nature Climate Change*, *3*(4),  
 439 369–373. Retrieved from <https://doi.org/10.1038/nclimate1716> doi:  
 440 [10.1038/nclimate1716](https://doi.org/10.1038/nclimate1716)
- 441 Lee, W.-L., & Liang, H.-C. (2019). *As-rcec taiesm1.0 model output prepared for*  
 442 *cmip6 cmip*. Earth System Grid Federation. Retrieved from [https://doi.org/10](https://doi.org/10.22033/ESGF/CMIP6.9684)  
 443 [.22033/ESGF/CMIP6.9684](https://doi.org/10.22033/ESGF/CMIP6.9684) doi: [10.22033/ESGF/CMIP6.9684](https://doi.org/10.22033/ESGF/CMIP6.9684)
- 444 Li, J., Miao, C., Wei, W., Zhang, G., Hua, L., Chen, Y., & Wang, X. (2021). Evalu-  
 445 ation of cmip6 global climate models for simulating land surface energy and water  
 446 fluxes during 1979–2014. *Journal of Advances in Modeling Earth Systems*, *13*(6),  
 447 e2021MS002515. Retrieved from [https://agupubs.onlinelibrary.wiley.com/](https://agupubs.onlinelibrary.wiley.com/doi/abs/10.1029/2021MS002515)  
 448 [doi/abs/10.1029/2021MS002515](https://agupubs.onlinelibrary.wiley.com/doi/abs/10.1029/2021MS002515) (e2021MS002515 2021MS002515) doi:  
 449 <https://doi.org/10.1029/2021MS002515>
- 450 Lovato, T., Peano, D., & Butenschön, M. (2021). *Cmcc cmcc-esm2 model output*  
 451 *prepared for cmip6 cmip*. Earth System Grid Federation. Retrieved from [https://](https://doi.org/10.22033/ESGF/CMIP6.13164)  
 452 [doi.org/10.22033/ESGF/CMIP6.13164](https://doi.org/10.22033/ESGF/CMIP6.13164) doi: [10.22033/ESGF/CMIP6.13164](https://doi.org/10.22033/ESGF/CMIP6.13164)
- 453 Lutsko, N. J., Baldwin, J. W., & Cronin, T. W. (2019, September). The Impact  
 454 of Large-Scale Orography on Northern Hemisphere Winter Synoptic Temper-  
 455 ature Variability. *Journal of Climate*, *32*(18), 5799–5814. Retrieved 2021-  
 456 10-29, from [https://journals.ametsoc.org/view/journals/clim/32/18/](https://journals.ametsoc.org/view/journals/clim/32/18/jcli-d-19-0129.1.xml)  
 457 [jcli-d-19-0129.1.xml](https://journals.ametsoc.org/view/journals/clim/32/18/jcli-d-19-0129.1.xml) doi: [10.1175/JCLI-D-19-0129.1](https://doi.org/10.1175/JCLI-D-19-0129.1)
- 458 Mahony, C., Wang, T., Hamann, A., & Cannon, A. (2021, 06). *A cmip6 en-*  
 459 *semble for downscaled monthly climate normals over north america*. doi:

- 460 10.31223/X5CK6Z
- 461 Nakamura, H., & Wallace, J. M. (1990, May). Observed Changes in Baro-  
 462 clinic Wave Activity during the Life Cycles of Low-Frequency Circulation  
 463 Anomalies. *Journal of the Atmospheric Sciences*, *47*(9), 1100–1116. Re-  
 464 trieved 2021-08-04, from [https://journals.ametsoc.org/view/journals/  
 465 atasc/47/9/1520-0469\\_1990.047\\_1100\\_ocibwa\\_2.0\\_co\\_2.xml](https://journals.ametsoc.org/view/journals/atasc/47/9/1520-0469_1990.047_1100_ocibwa_2.0_co_2.xml) doi: 10.1175/  
 466 1520-0469(1990)047<1100:OCIBWA>2.0.CO;2
- 467 O’Gorman, P. A., & Schneider, T. (2009). The physical basis for increases in  
 468 precipitation extremes in simulations of 21st-century climate change. *Proceed-  
 469 ings of the National Academy of Sciences*, *106*(35), 14773–14777. Retrieved  
 470 from <https://www.pnas.org/doi/abs/10.1073/pnas.0907610106> doi:  
 471 10.1073/pnas.0907610106
- 472 Park, S., & Shin, J. (2019). *Snu sam0-unicon model output prepared for cmip6 cmip*.  
 473 Earth System Grid Federation. Retrieved from [https://doi.org/10.22033/  
 474 ESGF/CMIP6.1489](https://doi.org/10.22033/ESGF/CMIP6.1489) doi: 10.22033/ESGF/CMIP6.1489
- 475 Reidmiller, D., Avery, C., Easterling, D., Kunkel, K., Lewis, K., Maycock, T., &  
 476 Stewart, B. (2018). *Impacts, risks, and adaptation in the united states: Fourth  
 477 national climate assessment* (Vol. 2; Tech. Rep.). Washington, DC, USA: U.S.  
 478 Global Change Research Program. doi: 10.7930/NCA4.2018.
- 479 Rupp, D. E., Abatzoglou, J. T., Hegewisch, K. C., & Mote, P. W. (2013). Evalua-  
 480 tion of cmip5 20th century climate simulations for the pacific northwest usa. *Jour-  
 481 nal of Geophysical Research: Atmospheres*, *118*(19), 10,884–10,906. Retrieved from  
 482 <https://agupubs.onlinelibrary.wiley.com/doi/abs/10.1002/jgrd.50843>  
 483 doi: <https://doi.org/10.1002/jgrd.50843>
- 484 Sillmann, J., Kharin, V. V., Zhang, X., Zwiers, F. W., & Bronaugh, D. (2013).  
 485 Climate extremes indices in the cmip5 multimodel ensemble: Part 1. model eval-  
 486 uation in the present climate. *Journal of Geophysical Research: Atmospheres*,  
 487 *118*(4), 1716–1733. Retrieved from [https://agupubs.onlinelibrary.wiley  
 488 .com/doi/abs/10.1002/jgrd.50203](https://agupubs.onlinelibrary.wiley.com/doi/abs/10.1002/jgrd.50203) doi: <https://doi.org/10.1002/jgrd.50203>
- 489 Swart, N. C., Cole, J. N., Kharin, V. V., Lazare, M., Scinocca, J. F., Gillett, N. P.,  
 490 ... Sigmond, M. (2019). *Cccma canesm5 model output prepared for cmip6 cmip*.  
 491 Earth System Grid Federation. Retrieved from [https://doi.org/10.22033/  
 492 ESGF/CMIP6.1303](https://doi.org/10.22033/ESGF/CMIP6.1303) doi: 10.22033/ESGF/CMIP6.1303
- 493 Tarek, M., Brissette, F. P., & Arsenault, R. (2020). Evaluation of the era5 re-  
 494 analysis as a potential reference dataset for hydrological modelling over north  
 495 america. *Hydrology and Earth System Sciences*, *24*(5), 2527–2544. Re-  
 496 trieved from <https://hess.copernicus.org/articles/24/2527/2020/> doi:  
 497 10.5194/hess-24-2527-2020
- 498 Tatebe, H., & Watanabe, M. (2018). *Miroc miroc6 model output prepared for  
 499 cmip6 cmip*. Earth System Grid Federation. Retrieved from [https://doi.org/  
 500 10.22033/ESGF/CMIP6.881](https://doi.org/10.22033/ESGF/CMIP6.881) doi: 10.22033/ESGF/CMIP6.881
- 501 Taylor, K. E., Stouffer, R. J., & Meehl, G. A. (2012). An overview of cmip5 and the  
 502 experiment design. *Bulletin of the American Meteorological Society*, *93*(4), 485 -  
 503 498. Retrieved from [https://journals.ametsoc.org/view/journals/bams/93/  
 504 4/bams-d-11-00094.1.xml](https://journals.ametsoc.org/view/journals/bams/93/4/bams-d-11-00094.1.xml) doi: 10.1175/BAMS-D-11-00094.1
- 505 Wehrli, K., Guillod, B. P., Hauser, M., Leclair, M., & Seneviratne, S. I. (2018). As-  
 506 sessing the dynamic versus thermodynamic origin of climate model biases. *Geo-  
 507 physical Research Letters*, *45*(16), 8471–8479. Retrieved from [https://agupubs  
 508 .onlinelibrary.wiley.com/doi/abs/10.1029/2018GL079220](https://agupubs.onlinelibrary.wiley.com/doi/abs/10.1029/2018GL079220) doi: [https://doi  
 509 .org/10.1029/2018GL079220](https://doi.org/10.1029/2018GL079220)
- 510 Wieners, K.-H., Giorgetta, M., Jungclaus, J., Reick, C., Esch, M., Bittner, M., ...  
 511 Roeckner, E. (2019). *Mpi-m mpiesm1.2-lr model output prepared for cmip6 cmip*.  
 512 Earth System Grid Federation. Retrieved from [https://doi.org/10.22033/  
 513 ESGF/CMIP6.742](https://doi.org/10.22033/ESGF/CMIP6.742) doi: 10.22033/ESGF/CMIP6.742

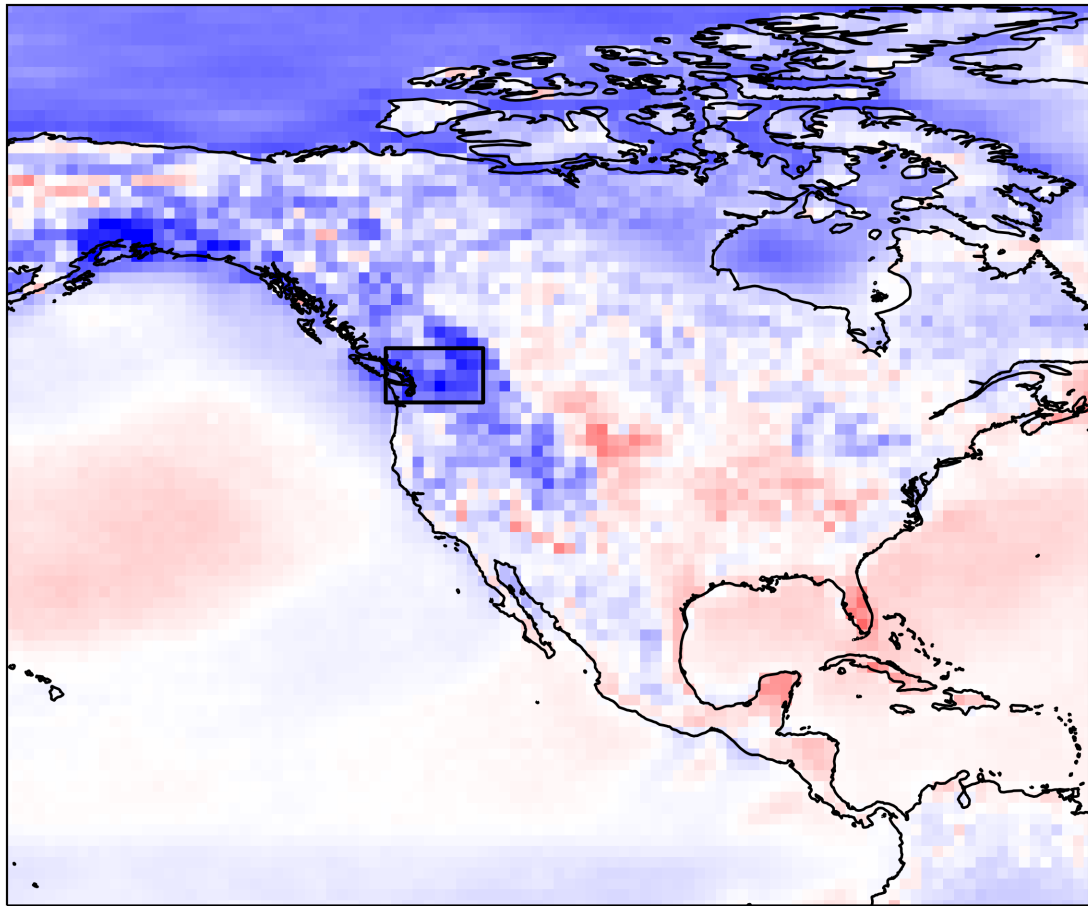
- 514 Wilcox, E. M., & Donner, L. J. (2007). The frequency of extreme rain events in  
515 satellite rain-rate estimates and an atmospheric general circulation model. *Jour-*  
516 *nal of Climate*, 20(1), 53 - 69. Retrieved from [https://journals.ametsoc.org/  
517 view/journals/clim/20/1/jcli3987.1.xml](https://journals.ametsoc.org/view/journals/clim/20/1/jcli3987.1.xml) doi: 10.1175/JCLI3987.1
- 518 Yukimoto, S., Koshiro, T., Kawai, H., Oshima, N., Yoshida, K., Urakawa, S., ...  
519 Adachi, Y. (2019). *Mri mri-esm2.0 model output prepared for cmip6 cmip*. Earth  
520 System Grid Federation. Retrieved from [https://doi.org/10.22033/ESGF/  
521 CMIP6.621](https://doi.org/10.22033/ESGF/CMIP6.621) doi: 10.22033/ESGF/CMIP6.621
- 522 Ziehn, T., Chamberlain, M., Lenton, A., Law, R., Bodman, R., Dix, M., ... Druken,  
523 K. (2019). *Csiro access-esm1.5 model output prepared for cmip6 cmip*. Earth  
524 System Grid Federation. Retrieved from [https://doi.org/10.22033/ESGF/  
525 CMIP6.2288](https://doi.org/10.22033/ESGF/CMIP6.2288) doi: 10.22033/ESGF/CMIP6.2288

## 526 **Acknowledgments**

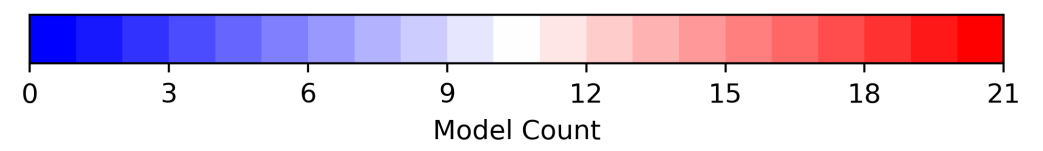
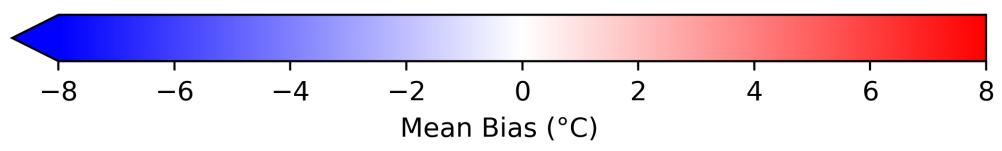
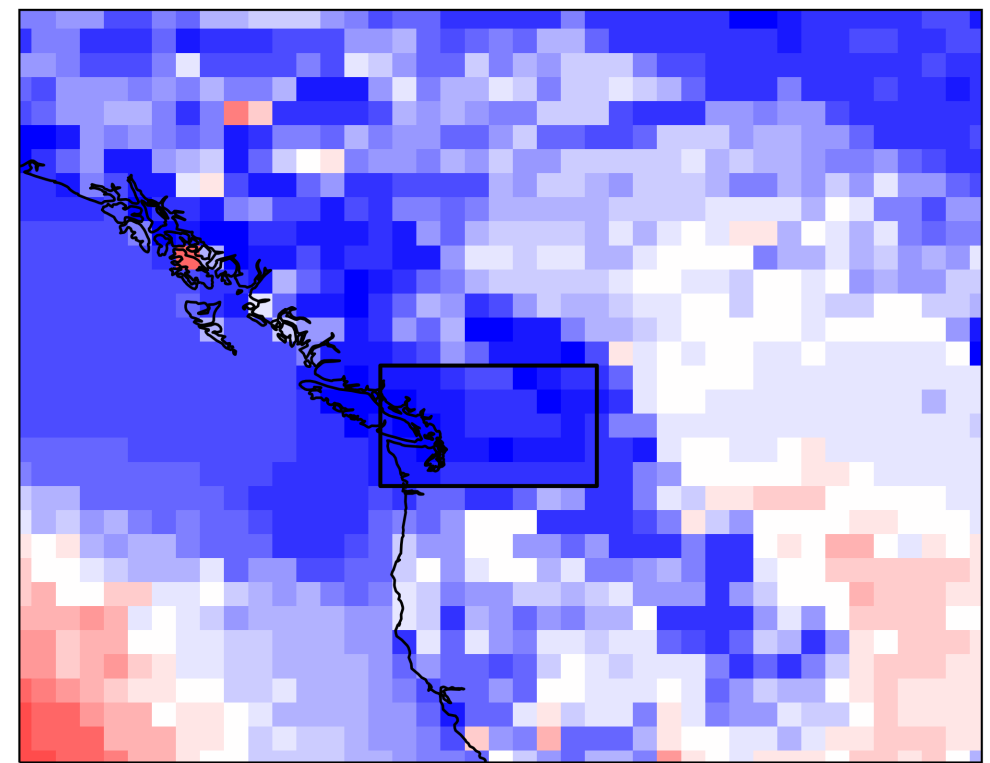
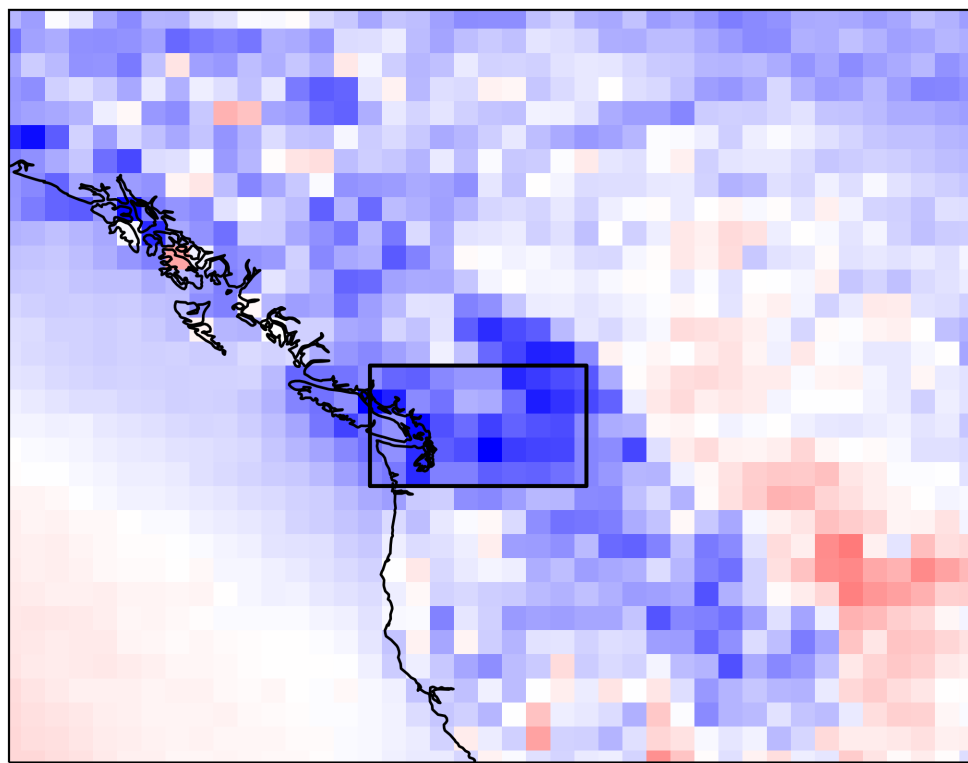
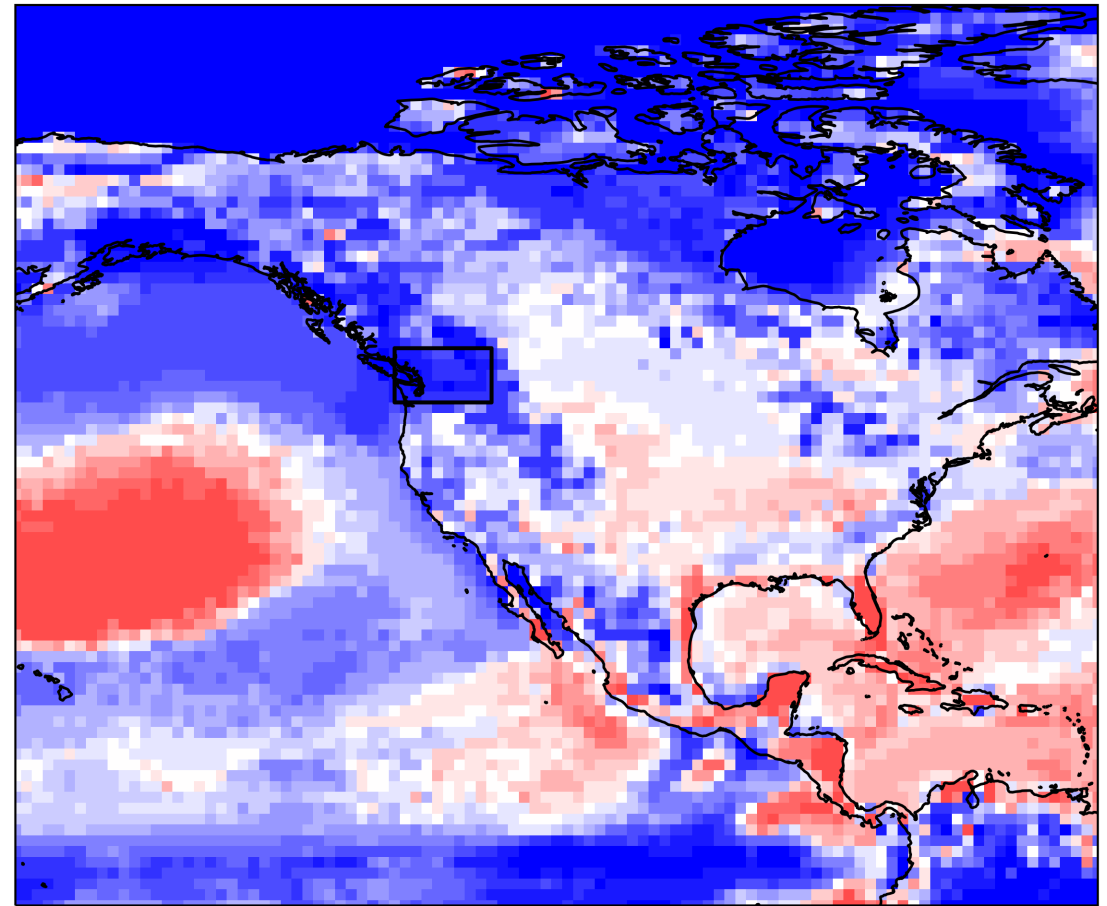
527 This work was supported by funding from the State of Washington. CMIP6 data was  
528 accessed using the Pangeo platform's data catalog (<https://pangeo.io>) Abernathey et al.  
529 (2017), which was supported by NSF Award 1740648. 152020Hersbach et al.Hersbach  
530 et al. () was downloaded from the Copernicus Climate Change Service (C3S) Climate  
531 Data Store.

CMIP6\_bias.png.

(a)

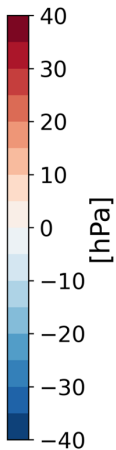
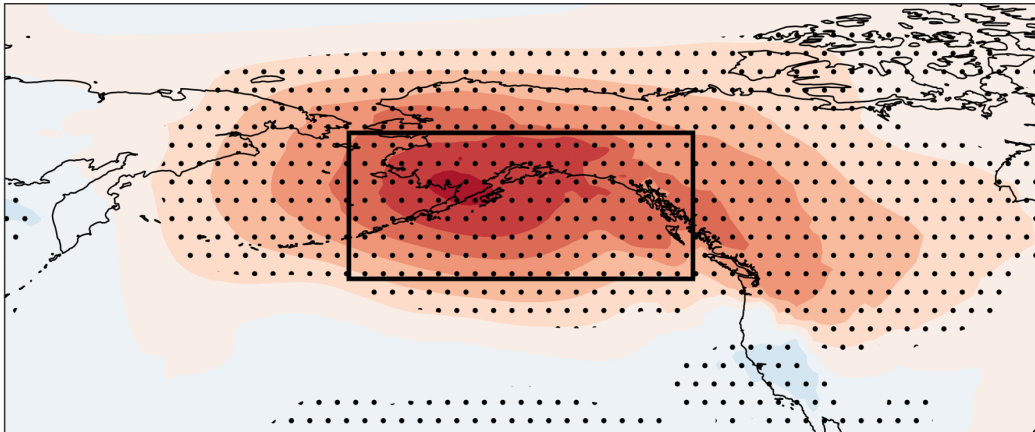


(b)

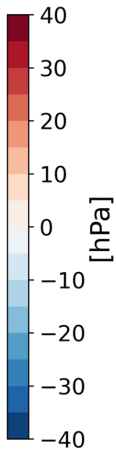
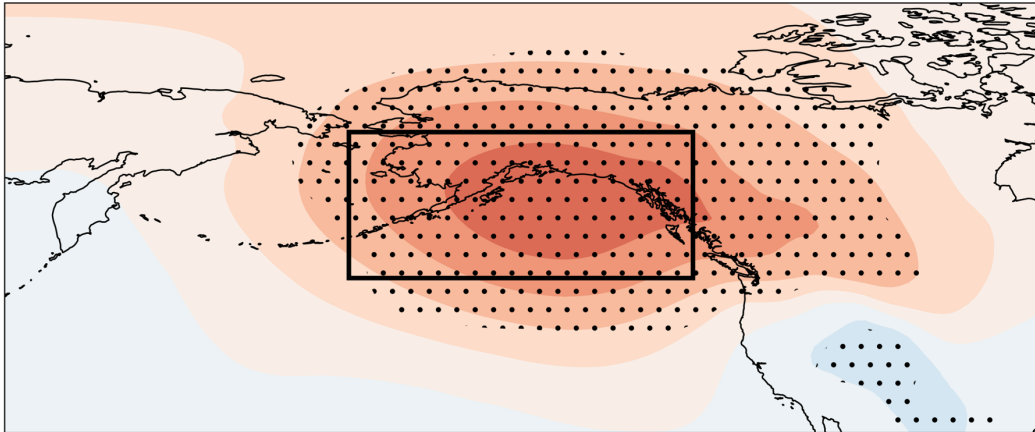


Composite\_SLP.png.

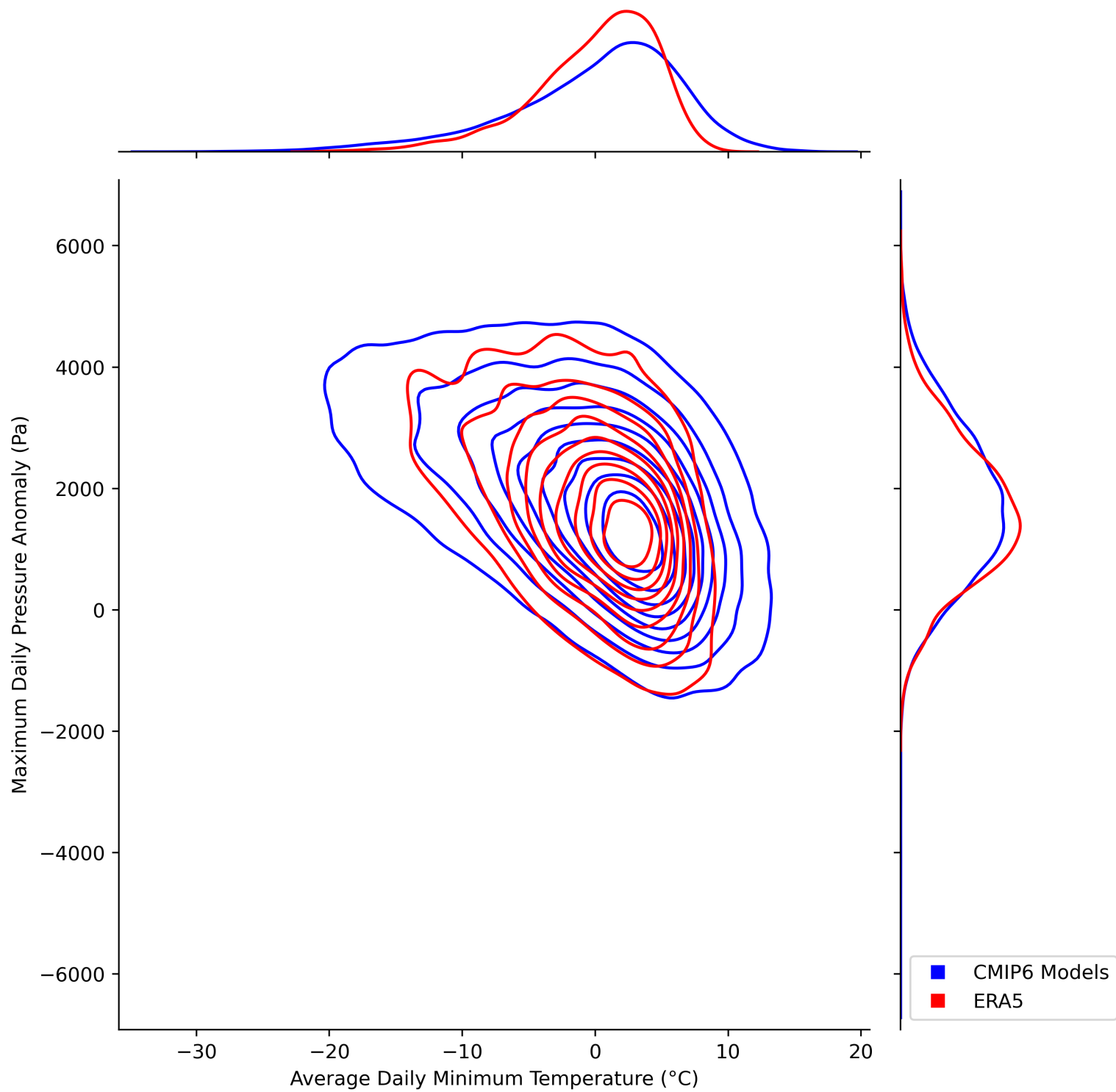
(a)



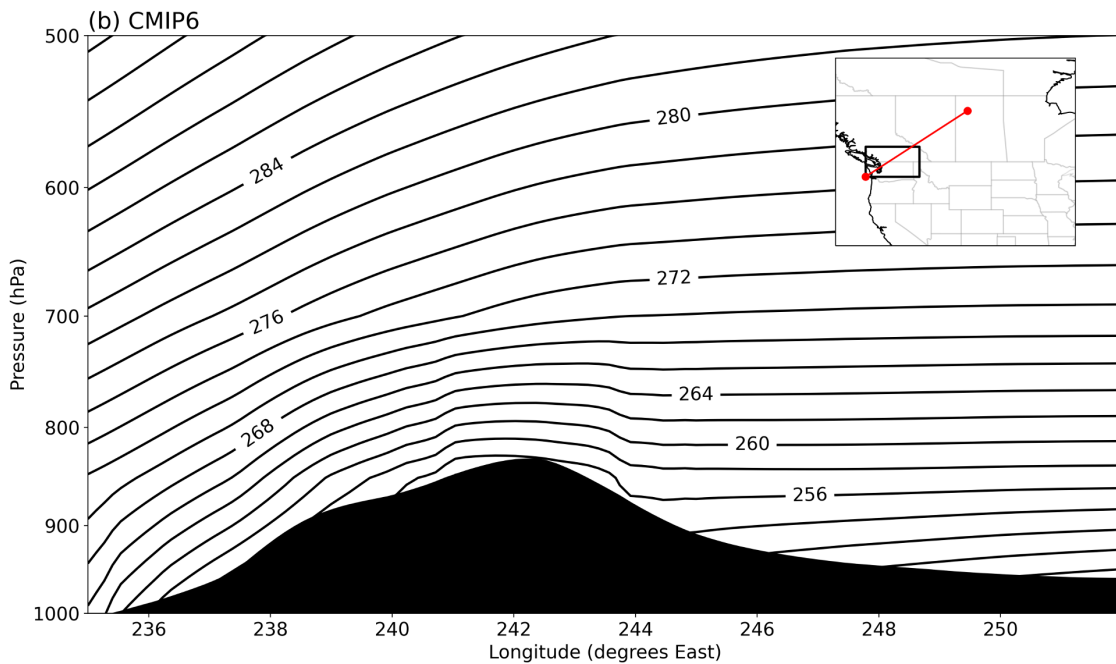
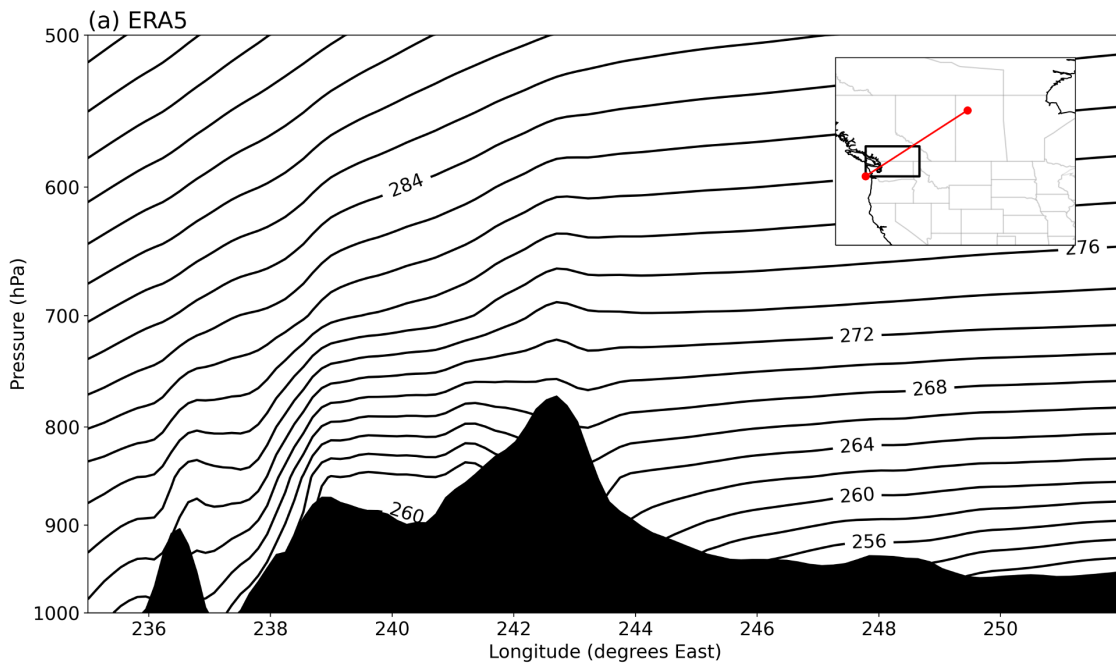
(b)



density.png.

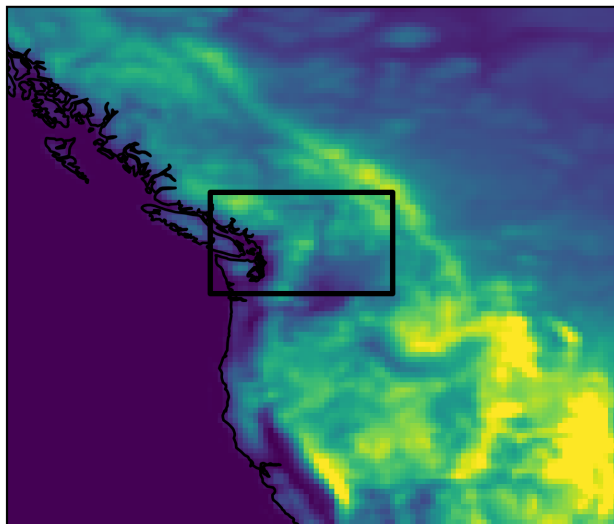


cross\_section.png.

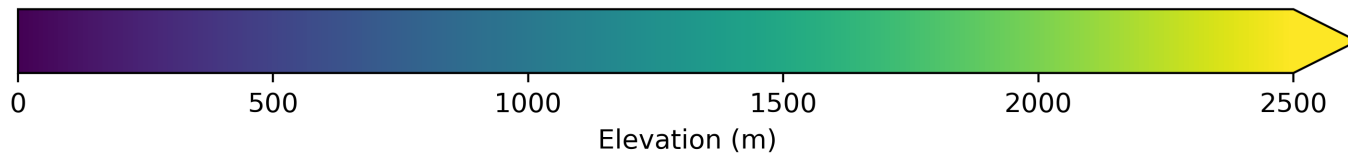
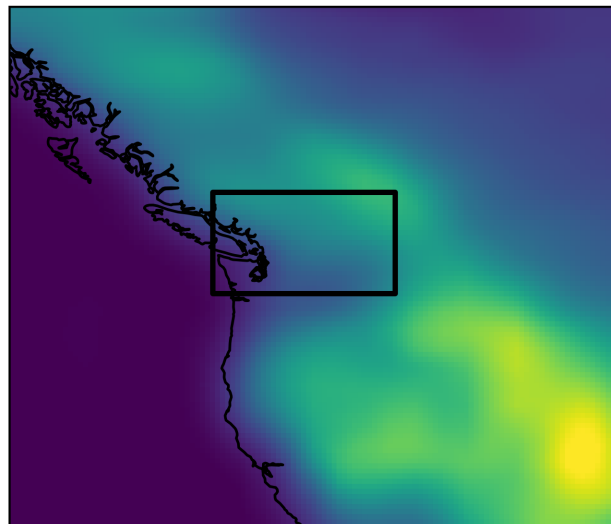


orography.png.

(a) ERA5

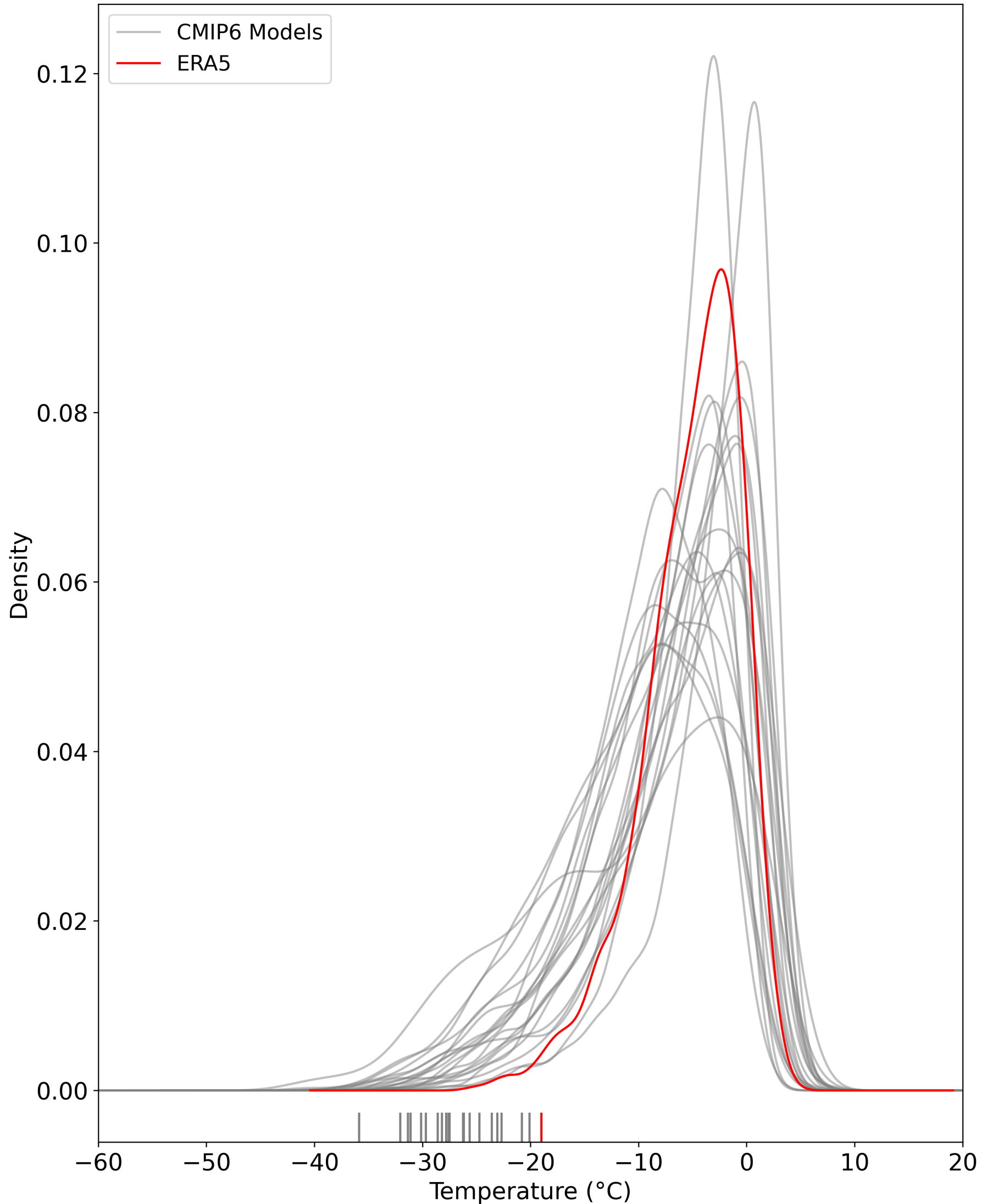


(b) CMIP6



tasmin\_bias.png.

(a)



(b)

